



# FASN inhibitor TVB-3166 prevents S-acylation of the spike protein of human coronaviruses

Katrina Mekhail<sup>1,2,\*</sup>, Minhyoung Lee<sup>1,2,\*</sup>, Michael Sugiyama<sup>3,\*</sup>, Audrey Astori<sup>4</sup>, Jonathan St-Germain<sup>4</sup>, Elyse Latreille<sup>2,5</sup>, Negar Khosraviani<sup>2</sup>, Kuiru Wei<sup>2</sup>, Zhijie Li<sup>1</sup>, James Rini<sup>1,6</sup>, Warren L. Lee<sup>1,2,5,7</sup>, Costin Antonescu<sup>3</sup>, Brian Raught<sup>4,8</sup>, and Gregory D. Fairn<sup>1,2,9,10,\*</sup>

<sup>1</sup>Department of Biochemistry, University of Toronto, Toronto, Ontario, Canada; <sup>2</sup>Keenan Research Centre, St. Michael's Hospital, Unity Health Toronto, Toronto, Ontario, Canada; <sup>3</sup>Department of Chemistry and Biology, Ryerson University, Toronto, Ontario, Canada; <sup>4</sup>Princess Margaret Cancer Centre, University Health Network, Ontario, Canada; <sup>5</sup>Department of Laboratory Medicine and Pathobiology, University of Toronto, Toronto, Ontario, Canada; <sup>6</sup>Department of Molecular Genetics, University of Toronto, Ontario, Canada; <sup>7</sup>Department of Medicine, University of Toronto, Toronto, Ontario, Canada; <sup>8</sup>Department of Medical Biophysics, University of Toronto, Ontario, Canada; <sup>9</sup>Department of Surgery, University of Toronto, Toronto, Ontario, Canada; <sup>10</sup>Department of Pathology, Dalhousie University, Halifax, Nova Scotia, Canada

**Abstract** The spike protein of severe acute respiratory syndrome coronavirus 2 (SARS-CoV-2) and other coronaviruses mediates host cell entry and is S-acylated on multiple phylogenetically conserved cysteine residues. Multiple protein acyltransferase enzymes have been reported to post-translationally modify spike proteins; however, strategies to exploit this modification are lacking. Using resin-assisted capture MS, we demonstrate that the spike protein is S-acylated in SARS-CoV-2-infected human and monkey epithelial cells. We further show that increased abundance of the acyltransferase ZDHHC5 associates with increased S-acylation of the spike protein, whereas ZDHHC5 knockout cells had a 40% reduction in the incorporation of an alkynyl-palmitate using click chemistry detection. We also found that the S-acylation of the spike protein is not limited to palmitate, as clickable versions of myristate and stearate were also labelled the protein. Yet, we observed that ZDHHC5 was only modified when incubated with alkyne-palmitate, suggesting it has specificity for this acyl-CoA, and that other ZDHHC enzymes may use additional fatty acids to modify the spike protein. Since multiple ZDHHC isoforms may modify the spike protein, we also examined the ability of the FASN inhibitor TVB-3166 to prevent S-acylation of the spike proteins of SARS-CoV-2 and human CoV-229E. We show that treating cells with TVB-3166 inhibited S-acylation of expressed spike proteins and attenuated the ability of SARS-CoV-2 and human CoV-229E to spread in vitro. Our findings further substantiate the necessity of CoV spike protein S-acylation and demonstrate that de novo fatty acid synthesis is critical for the proper S-acylation of the spike protein.

**Supplementary key words** S-acylation • ZDHHC • spike coronavirus • click chemistry • FASN • palmitate • SARS-CoV-2 • CoV-229E • host cell entry • infection

Since 2003, coronaviruses (CoVs) have resulted in three zoonotic outbreaks: severe acute respiratory syndrome coronavirus (SARS-CoV) in 2003, Middle East respiratory syndrome in 2012, and SARS-CoV-2 in December 2019 (1, 2). CoVs infect humans and animals and cause various diseases targeting different tissues, including respiratory, enteric, renal, and hepatic (3, 4). The current pandemic highlights the need for effective treatments of this family of viruses. There are enormous efforts to develop prophylaxis and therapeutic options for SARS-CoV-2, including vaccination, protease inhibitors, and soluble decoy receptors (5–7). Many putative countermeasures target the spike protein, which is required to attach the virus to cells via binding to the angiotensin-converting enzyme 2 (ACE2) and potentially other host proteins (6). Further, spike protein proteolytic cleavage generates an S2 fragment capable of stimulating viral fusion and payload delivery into the cytosol (8). However, the high mutation rates of positive-sense (+) RNA viruses may result in resistance to some of these therapeutic approaches (9, 10). In addition, many potential zoonotic CoV species in bat and civet populations necessitate exploring all available therapies (11, 12). Thus, identifying a pan-CoV infection therapy that targets a host enzyme is desirable for current and future potential zoonotic infections.

Although not truly synonymous, S-palmitoylation or S-acylation is often used interchangeably to describe the reversible covalent addition of palmitoyl or other fatty acyl chains to cysteine (Cys) residues via a thioester bond. This modification can occur spontaneously in high concentrations of acyl-CoAs or catalyzed by a

\*These authors contributed equally to this work.

\*For correspondence: Gregory D. Fairn, [gfairn@dal.ca](mailto:gfairn@dal.ca).



family of zinc finger Asp-His-His-Cys-containing protein acyltransferases or simply ZDHHC enzymes. In the Spring of 2020, Krogan *et al.* (13) reported that ZDHHC5 and its binding partner Golga7 interact with the spike protein of SARS-CoV-2 using an affinity purification/MS approach. The results suggest that the cytosolic tail of the spike protein may be post-translationally S-acylated. A variety of laboratories have substantiated this, and collectively, these studies have demonstrated that multiple protein acyltransferases, including ZDHHC2, 3, 5, 6, 8, 9, 11, 12, 20, 21, and 24, directly or indirectly influence the S-palmitoylation/acylation of the spike protein depending on the cellular context (14–20). These findings likely result from the lack of specificity of some ZDHHC enzymes and the promiscuous nature of some substrates. Considering that the spike protein contains 10 Cys residues in proximity to the membrane, this would only increase the chances of modification by various transferases.

Previously, the spike protein of the murine hepatitis virus (MHV) required S-acylation of its C-terminal tail to support virion production (21). Specifically, preventing S-acylation prevented the MHV spike protein from being incorporated into new virions (21). Furthermore, a mutant version of spike unable to be S-palmitoylated displayed a reduced ability to stimulate membrane fusion vis-à-vis syncytium formation (21, 22). In addition, S-acylation of the SARS-CoV spike is critical for its ability to catalyze cell-cell fusion (23). Here, we aimed to extend the findings and investigate the role of ZDHHC5 in spike S-acylation and its role in the human cold virus CoV-229E. Given the large number of ZDHHC enzymes that may potentially S-acylate the spike protein, we also sought to examine the ability of the FASN inhibitor TVB-3166 (Sigma) to limit S-acylation.

## MATERIALS AND METHODS

### Reagents

TVB-3166 (catalog no.: SML1694), 2-bromohexadecanoic acid (catalog no.: 238422), EDTA-free protease inhibitor (catalog no.: 1183617001), Tris(2-carboxyethyl)phosphine (catalog no.: C4706), and tert-butanol (catalog no.: 471712) were purchased from Millipore-Sigma (Oakville, Canada). Phusion polymerase, XhoI and NheI FastDigest restriction enzymes, T4 DNA ligase, dithiobissuccinimidyl propionate (DSP), Protein G Sepharose, Lipofectamine 3000, RNAiMAX, Eagle's MEM (EMEM), and SuperSignal West Pico were purchased from Thermo Fisher Scientific (Mississauga, Canada). DMEM, Temin's modified Eagle's medium (catalog no.: 11935046), FBS, charcoal-stripped FBS, and trypsin/EDTA were obtained from Wisent Bio Products (St. Bruno, Canada). Triton X-100, DMSO, and CuSO<sub>4</sub> were from BioShop Canada, Inc (Burlington, Canada), alkynyl-palmitate (Click Chemistry Tools, Scottsdale, AZ), cyanine 5.5 (Cy5.5) (tetramethylindolyl)(di)-carbocyanines; Cyanine-azide (Lumiprobe, Hunt Valley, MD), Site Counter (Badrilla, Leeds, UK), and paraformaldehyde (PFA) (Electron Microscope Science, Hatfield, PA).

### Plasmids

pcDNA3.1-SARS-CoV-2-spike (Addgene plasmid #145032), pCEP4-myc-ACE2 (Addgene plasmid #141185), PBcmv-229E-wt\_WRPE (24), hemagglutinin (HA)-tagged ZDHHC5 (25), EGFP-Cl (Clontech), and mCherry-Cl (Clontech). The 229E spike complementary DNA was amplified by PCR with the forward primer: 5'-TTTTTTGCGGCTAGCATGTTTCGTGCTGCTGG and the reverse primer: 5'-TTTTTTGCGCTCGAGTCACGCCGCGCCACCTGGCTGGTTTCGGTCTGGA TGTGGATCTTTTCCA using Phusion polymerase (New England Biolabs) according to the manufacturer's instruction. The amplified 229E sequence and SARS-CoV-2 S plasmid were incubated with XhoI and NheI restriction enzymes at 37°C for 1 h. The reactions were then heat-inactivated and purified with a PCR clean-up kit. The insert and vector were then incubated with T4 DNA ligase at 16°C overnight. The ligation mixture was transformed into NEB 5-alpha high-efficiency *Escherichia coli* and plated on LB plates with the appropriate antibiotic. Plasmids were then harvested with a midi prep kit following the manufacturer's instructions.

### Mutagenesis of SARS-CoV-2 spike multi-Cys to serine

The SARS-CoV-2 spike protein has 10 Cys residues in its cytosolic tail; C1235, C1236, C1240, C1241, C1243, C1247, C1248, C1250, C1253, and C1254. In this study, all 10 Cys residues were replaced by Ser. Sequential PCR and overlap extension PCR were used for the complete substitution strategy. Using pcDNA3.1 SARS-CoV-2 Spike-C9 as an initial template, two fragments were generated: 5'-terminal and 3'-terminal fragments. To amplify the 3'-terminal fragment (containing 10 Cys to Ser mutation), three sequential PCRs were performed using overlapping forward primers (F2 primer overlaps with F1 primers, F3 primer overlaps with F2 primers). As a result, fragment 1 served as a DNA template for fragment 2, and fragment 2 served as a template for fragment 3. The fragments 1, 2, and 3 were generated using forward primers F1-5'-CTCCTCCTCCTCCGGCAGCTCCTCCAAGTTCGATGAGGACGATAG-3', F2-5'-CCTCCTCCTCCAGCTCCTGAAGGGCTCCTCCTCCTCCGGCAGCT-3', and F3-5'-TGATGGTGA CCATCATGCTGTCTCTCCATGACCTCCTCCTCCAGCTCC CTG-3', respectively, and reverse primer 5'-TCTAGACTCG AGCTAAGCGGGAGC-3'. To amplify the 5' DNA fragment, forward primer 5'-CAAGCTGGCTAGCATGTTTGTCTT CC-3' and reverse primer 5'-TCATGGAGGACAGCATGAT GGTACCATCA-3' were used. The 5' DNA fragment and 3'DNA fragment were annealed together with their complementary overhanging by PCR using the primer pairs 5'-CA AGCTGGCTAGCATGTTTGTCTTCC-3' and 5'-TCTAGAC TCGAGCTAAGCGGGAGC-3' to generate full-length DNA. All PCR thermocycler conditions were based on Touchdown PCR (26). The multisite mutated SARS-CoV-2 spike was then subcloned into the pcDNA3.1 vector using NheI and XhoI restriction digestion.

### Cell culture

Human embryonic kidney 293T (HEK293T) cells were cultured in DMEM supplemented with 10% FBS at 37°C and 5 CO<sub>2</sub>. MRC-5 cells (ATCC) were cultured in EMEM supplemented with 10% FBS and 1% penicillin/streptomycin (Gibco).

### Syncytium formation assay

HEK293T cells were seeded in 6-well plates and transfected with EGFP-Cl vector with myc-ACE2 vector and mCherry-Cl

vector with CoV-2 Spike-C9 or spike multi-Cys to serine mutant. After 16–24 h of incubation, cells were lifted by trypsinization and cocultured overnight. Fluorescent images were acquired through EVOS FLoid™ Cell Imaging System.

### Antibodies and antibody-conjugated beads

C9 antibody (Clone 1D4; Santa Cruz; catalog no.: sc-57432), anti-C9 agarose bead (Cube Biotech), HA antibody (Abcam; catalog no.: ab9110), SARS-CoV-2 (coronavirus disease 2019 [COVID-19]) spike RBD antibody (GenTex; catalog no.: HL257), ZDHHC5 antibody (Sigma; catalog no.: HPA014670), and fluorescent secondary antibodies (Jackson Laboratories, Invitrogen, LI-COR).

### siRNA transfection

MRC-5 cells seeded on 6-well tissue culture plates were transfected 2x, 24 h apart, followed by a 24 to 48 h recovery before infection with 229E. Cells were initially transfected at 50% confluence in 1 ml Opti-MEM Reduced-Serum Medium (Gibco). An siRNA transfection master mix of Lipofectamine RNAiMAX, siRNA (CTRL or ZDHHC5), and Opti-MEM was made according to the manufacturer's instructions, with a final siRNA concentration of 50 nM. Cells were transfected with the siRNA master mix for 4 h, followed by a change to growth media. After the last transfection, media were changed to growth media and cells were given 24 to 48 h recovery before the infection, at which point they were at 100% confluence. Oligo sequences used CTRL nontargeting siRNA: CGUACUGCUUGCGAUACGGUU and ZDHHC5 siRNA: CUGUGAAGAUGCAUGGAUAAUU (27).

### Immunoblotting

SDS polyacrylamide gels were transferred on PVDF membranes by Trans-blot Turbo System at 25 V for 20 min. Membranes were blocked with 5% BSA for 1 h at room temperature and incubated with primary antibodies diluted in blocking solution at 4°C overnight (anti-C9; Santa Cruz). Membranes were washed with TBS-0.1% Tween-20 for 5 min, three times, and incubated with appropriate secondary antibodies. Blots were then washed three times with TBS-0.1% Tween-20 for 5 min each wash. The membranes were treated with ECL and imaged with ChemiDoc Imaging System (Bio-Rad).

### Coimmunoprecipitation

HEK293T cells seeded in T25 flask (25 cm<sup>2</sup>) were grown until reaching 70–90% confluency. According to the manufacturer's instruction, cells were transfected with 3xHA-ZDHHC5 and CoV-2 Spike-C9 plasmids using Lipofectamine 3000 and incubated for 16–24 h. For protein crosslinking, cells were incubated with a 2 mM DSP crosslinker in PBS at 4°C for 2 h. DSP was quenched in 20 mM glycine in PBS for 15 min, and cells were lysed in NP-40 lysis buffer (20 mM Tris and adjusted to pH 7.4, 150 mM NaCl, 1% NP-40, and 2 mM EDTA) supplemented with cOmplete Protease Inhibitor Cocktail tablet (Roche), EDTA-free at a constant agitation for 30 min at 4°C. Cell lysates were centrifuged at 12,000 g for 20 min, and the supernatant was collected. Samples were precleared by incubating with protein G Sepharose beads and spun at 14,000 g for 1 min to collect the supernatant. Precleared samples were incubated with anti-C9 or anti-HA primary antibodies overnight at 4°C. To form a primary antibody-bead complex,

Protein G beads were added and incubated for 30 min. Beads were washed in cold wash buffer (20 mM Tris, pH 7.4, 350 mM NaCl, 1% NP-40, and 2 mM EDTA) six times, and proteins were eluted with SDS Laemmli buffer and heated for 30 min at 37°C before SDS-PAGE.

### Immunofluorescence

Cells were seeded on an 18 mm round coverslip in a 12-well plate. Cells expressing Spike-C9 or spike<sup>C>S</sup>-C9 ectopically were washed with PBS and then fixed with 4% PFA. The remaining PFA was quenched by 0.15 M glycine for 20 min at room temperature. Cells were blocked with 5% BSA in PBS for 1 h and probed with a primary antibody (SARS-CoV-2 spike RBD; GenTex) in 5% BSA for 1 h. Cells were washed with PBS and probed with fluorescently labeled secondary antibodies for 1 h.

### Confocal microscopy

Imaging in the St. Michael's Hospital BioImaging was conducted using an Andor Diskcovery multimodal imaging system provided by Quorum Technology (Guelph, Ontario). The system is based on a Leica DMI8 equipped with a 63x/1.47 numerical aperture oil objective; 405, 488, 561, and 637 nm laser lines; 450/50, 525/50, 600/50, 610/75, and 700/75 emission filters. Images were acquired using Metamorph software on a Hamamatsu ORCA-Flash 4.0 V2 sCMOS camera. Imaging at Ryerson University was performed on the Quorum WaveFX spinning disc based on an inverted Leica DMI8 equipped with an Andor Zyla 4.2 sCMOS camera using a 10x objective controlled by MetaMorph.

### Metabolic labeling/on-bead click chemistry assay

HEK293T cells seeded in T25 flask (25 cm<sup>2</sup>) were transfected with pcDNA3.1-SARS-CoV-2-Spike-C9 and incubated overnight in DMEM supplemented with 10% (v/v) charcoal-stripped FBS with or without 100 μM of clickable fatty acid analogs (Click Chemistry Tools) coupled to albumin. After 2 h or 18 h of labeling, cells were washed twice with ice-cold PBS and collected following scraping. Cells were lysed in immunoprecipitation buffer (20 mM Tris and adjusted to pH 8.0, 137 mM NaCl, 1% NP-40, and 2 mM EDTA) supplemented with EDTA-free cOmplete Protease Inhibitor Cocktail tablet and immunoprecipitated using C9-agarose beads (Cube Biotech) at 4°C overnight. The beads were then washed with ice-cold Dulbecco's PBS (D-PBS) 4 times and incubated in D-PBS supplemented with 1 μM Cy5.5-azide (Click Chemistry Tools), 1 mM Tris(2-carboxyethyl)phosphine (adjusted to pH 7.0), 1 mM CuSO<sub>4</sub>, 0.1 mM Tris((1-benzyl-4-triazolyl)methyl)amine (1:4 v/v DMSO:tert-Butanol) for 2 h. The beads were washed five times with D-PBS, and proteins were eluted with 5x SDS Laemmli buffer. Protein samples were resolved by SDS-PAGE and subjected to in-gel fluorescence using the 685–700 nm laser on the Li-Cor Odyssey Infrared Imaging System. Gels were later transferred to PVDF membranes for immunoblotting, as previously indicated.

### Flow cytometry

HEK293T cells seeded in T25 flask (25 cm<sup>2</sup>) were transfected with pcDNA3.1 SARS-CoV-2-Spike-C9 or pcDNA3.1 SARS-CoV-2-Spike-C9<sup>C>S</sup> and incubated overnight in DMEM supplemented with 10% (v/v) FBS. Cells were washed with PBS and then gently detached with 10 mM EDTA (pH = 7). Cells



were collected by centrifugation at 1,500 rpm for 5 min and then resuspended in flow buffer (PBS supplemented with 2% [v/v] FBS). About  $1 \times 10^6$  cells were then immunolabeled with primary antibody (SARS-CoV-2 spike RBD) in flow buffer for 30 min at 4°C. Cells were washed three times with flow buffer and then incubated with a secondary antibody. Cells were washed in flow buffer, and 4',6-diamidino-2-phenylindole (DAPI) was added to cells right before acquisition with the DB LSRFortessa™ X-20 Cell Analyzer. Analysis was completed on the FlowJo software (BD Biosciences).

### Acyl-polyethylene glycol exchange assay

HEK293T cells were seeded in 6-well plates in DMEM + 10% FBS and transfected with Lipofectamine 3000 reagent. For each well, 2.5 mg of either 229E Spike-C9 + HA-ZDHHC5, 229E Spike-C9 + EGFP-C1, SARS-CoV-2 Spike-C9 and HA-ZDHHC5, or SARS-CoV-2 Spike-C9 + EGFP-C1 DNA mixtures were diluted in Opti-MEM and mixed with Lipofectamine 3000 according to the manufacturer's instructions. Upon transfection, cells were treated with 0.2  $\mu$ M or 20  $\mu$ M of TVB-3166 or 50  $\mu$ M 2-BP. About 16 to 18 h post-transfection, cells were lysed and processed with the Site-Counter™ S-palmitoylated protein kit following the manufacturer's instructions. Samples were subjected to SDS-PAGE by resolving on a 3–8% Criterion™ XT Tris-Acetate gel (Bio-Rad) for immunoblotting.

### Propagation of the human 229E CoV

Human CoV 229E (ATCC® VR-740™) was purchased from ATCC (Manassas, VA). Stocks of the 229E virus were produced by propagation in MRC-5 cells. Briefly, a T75 flask of 90% confluent MRC-5 cells was infected with a multiplicity of infection (MOI) of 0.01 for 2 h at 33°C in infection media for viral adsorption. Unbound virus was removed by washing cells 2× with infection media, and infected cells were returned to the 33°C incubator in 12 ml infection media for 72 h. The virus-containing supernatant was centrifuged at 1,000 *g* for 5 min to remove cellular debris, and single-use aliquots of the virus were frozen at –80°C.

### Human CoV 229E plaque-forming unit assay

Plaque-forming unit assays were used to determine viral titers and experiments using protocols adapted from previous publications field (28, 29). Briefly, MRC-5 cells seeded on 6-well tissue culture and grown to 100% confluency in EMEM + 10% FBS + 1% PenStrep. Plates were infected with serially diluted virus in infection media (EMEM + 2% FBS + 1% PenStrep) for 1 h at 33°C in a volume of 300  $\mu$ l with periodic agitation. After virus adsorption, the unbound virus was removed by washing with infection media followed by agarose overlay with 1× MEM Temin's modification (Thermo Fisher; catalog no.: 11935046) + 0.3% agarose. Cells were then returned to the 33°C incubator until they showed obvious signs of cytopathic effects (typically 4–7 days postinfection), upon which plates were fixed with 10% neutral-buffered formalin for 4 h, followed by removal of the agarose plug and staining with 1% crystal violet for 15 min. Plaques were counted based on standard protocols for determining viral titer.

### Liquid viral infection assay

MRC-5 cells were seeded on glass coverslips and transfected. Cells were infected with 229E at an MOI of 0.005 for

2 h in a total volume of 2 ml per well. After virus adsorption, cells were washed 2× with infection media and then replaced with 2 ml infection for incubation at 33°C. After 72 h, cells were fixed with 4% PFA for 1 h, followed by 0.15% glycine, 0.1% Triton X-100, and 3% BSA for 15 min each. Cells were then incubated in a 1:50 dilution of mouse anti-229E spike protein antibody by inverted drop for 1 h at room temperature. After washing, cells were incubated in 1:1000 anti-mouse Alexa Fluor 488 secondary antibody (Jackson ImmunoResearch) and DAPI (1 mg/ml) for 1 h at room temperature, followed by mounting on slides with DAKO mounting media. Images were acquired with the WaveFX system. The total fluorescent signal was quantified with ImageJ (National Institutes of Health).

### SARS-CoV-2 infection and immunofluorescence

293A2T2 (HEK293 expressing ACE2 and TMPRSS2 ectopically) cells were grown in DMEM supplemented with 10% heat-inactivated FBS. About 20,000 cells were plated on coverslips in a 24-well plate the day before infection and infected with SARS-CoV-2 strain SB3 (30) at an MOI of 0.1 in DMEM for 1 h. Infectious media were changed with DMEM-2% FBS, and cells were incubated at 37°C at 5% CO<sub>2</sub>. For TVB treatment, at 6 h postinfection, the supernatant was replaced with fresh media DMEM-2% FBS containing either DMSO or the TVB compound at 0.1 or 1  $\mu$ M final concentration. Cells were incubated for 18 h at 37°C, with 5% CO<sub>2</sub>. After infection, cells were fixed with 4% PFA for 1 h at room temperature. After PFA fixation, cells were washed with PBS and permeabilized for 10 min with 0.1% Triton X-100. Cells were blocked in 2% BSA in PBS for 1 h before incubation with the primary antibody overnight at 4°C. Primary antinucleocapsid antibody (SARS-CoV-2 Nucleocapsid Antibody [HC2003]; catalog no.: A02039; GenScript) was used at 1:1,000 dilution. After removing the antibody solution, cells were washed in PBS and incubated for 1 h with secondary anti-human FITC (Bio-Legend) at room temperature. Cells were washed in PBS, and coverslips were mounted with Duolink in situ mounting medium with DAPI (Sigma; catalog no.: DUO82040). Cells were imaged using UPlan FL 40×/0.75 numerical aperture on a Yokogawa CSU-10 Spinning-disk confocal microscope. Images were processed using the Volocity Viewer, v.6 (Perkin Elmer).

### MHV-S infection of mice

Four-week-old female A/J mice were purchased from Jackson Laboratories. Mice were housed in the St. Michael's Hospital Vivarium on a standard light/dark cycle and were given free access to food and water. Before infection, mice were acclimatized for 1 week. Mouse infection experiments were performed in the dedicated BSL-2 room in the vivarium in accordance with the St. Michael's Hospital Animal Care Committee guidelines for animal use; approved animal protocol (ACC962, St. Michael's Hospital). One day prior to infection, the necks of mice were shaved, and chemical depilatory cream was used to remove all hair to obtain optimal oxygen saturation measurements during the study. For infection, mice were sedated with 5% isoflurane and infected intranasally with 150,000 units determined using a tissue culture infectious dose at 50%/mouse of MHV-S (Cedarlane; VR-766), which is known to induce pneumonitis (31). The virus was diluted in PBS to a final volume of 75  $\mu$ l before administration. After infection, mice were allowed to recover for 10 min in a cage on a covered heating pad. On the day of infection, TVB-3166 (SML1694) was reconstituted by adding a small

volume of DMSO (10% of the final volume) to the vial. The vial was briefly vortexed and heated in a 37°C water bath, and then corn oil was added to make a 5 mg/ml solution for treatments. Following recovery, mice were randomly separated into weight-matched groups and immediately received solvent control or TVB-3166 (30 mg/kg) by oral gavage. For the remainder of the study, mice were monitored daily and received one dose of TVB-3166 or solvent control per day. As previously reported (32), mice were sacrificed if they reached two of four end points: weight loss of 30% of the initial weight, body temperature below 31°C, oxygen saturation below 75%, or activity level of 1 (moribund). To measure oxygen saturation on awake mice, the Mouse Ox Plus device and software from Starr Life Sciences were used.

### Acyl-resin-assisted capture assay

HEK293 A2T2 and African green monkey VeroE6 cells were infected with SB3 SARS-CoV-2 for 24 h at an MOI of 0.5. Cells were harvested and lysed (1% Triton X-100, 50 mM Tris-HCl [pH 7.5], 150 mM NaCl, 1 mM EDTA, 1% SDS, 0.5% sodium deoxycholate, 100 µl mammalian protease inhibitor cocktail [Sigma; catalog no.: P8340], 5 µl Turbonuclease [BioVision; catalog no.: 9207-50KU], 10 mM *N*-ethylmaleimide [NEM; BioShop; catalog no.: ETM222.5]). Lysates were sonicated and incubated at 4°C on an end-over-end rotator for 1 h. Additional NEM was added to a final concentration of 20 mM, and samples were incubated for an additional hour on an end-over-end rotator at room temperature. Next, NEM was removed via methanol chloroform precipitation, and protein pellets were rinsed with methanol and air-dried. Pellets were resuspended in acyl-resin-assisted capture (RAC) binding buffer (100 mM Tris-HCl [pH 7.5], 1 mM EDTA, 1% SDS) by sonication. Hydroxylamine (NH<sub>2</sub>OH, 400 mM final concentration; or NaCl for control samples) was added before incubation with 30 µl of packed acyl-RAC beads (High-Capacity Acyl-RAC S3 beads; Nanocs; catalog no.: AR-S3-1,2) for 2 h at room temperature. Next, beads were washed three times with binding buffer and 10 times with NH<sub>4</sub>HCO<sub>3</sub> (50 mM, pH 8.3). Direct digestion on beads was performed using trypsin/Lys-C (1 µg per sample in 50 mM NH<sub>4</sub>HCO<sub>3</sub>, pH 8.3) for 5 h at 37°C on an end-over-end rotator. Beads were rinsed with 50 mM NH<sub>4</sub>HCO<sub>3</sub> (pH 8.3), and supernatant fractions were pooled. Samples were desalted and lyophilized before LC-MS analysis.

### LC-MS

LC-MS analysis was performed as previously described (33). Briefly, HPLC was performed on samples reconstituted in HCOOH (0.1%) and loaded on a 20 mm precolumn (C18 Acclaim PepMap™ 100, 75 µm × 2 cm, 3 µm, 100 Å; Thermo Fisher Scientific) and separated on a 50 mm analytical column (C18 Acclaim PepMap™ RSLC, 75 µm × 50 cm, 3 µm, 100 Å; Thermo Fisher Scientific) over a 2-h reversed-phase gradient (5–30% CH<sub>3</sub>CN in 0.1% HCOOH) with 250 nl/min flow rate on an EASY-nLC1200 pump in-line with a Q-Exactive HF mass spectrometer (Thermo Fisher Scientific) operated in positive-ion mode ESI. MS scans were performed at a resolution of 60,000 (full width at half maximum), followed by up to 20 MS/MS scans (higher-energy C-trap dissociation, 15,000 full width at half maximum) of the most intense parent ions. Dynamic exclusion (within 10 ppm) was set for 5 s.

### MS data processing

For the sequence database search, Thermo raw files (.raw) were converted to the .mzML format using Proteowizard

(version 3.0.19311), then searched using X!Tandem (v2013.06.15.1) and Comet (2014.02 rev. 2) against Chlorocebus sabaeus RefSeq (GCF\_015252025.1, v102; 61,745 entries) for the VeroE6 samples or Human RefSeq (v104; 36,113 entries) for the HEK293-A2T2 samples. Both databases were supplemented with the SARS-CoV-2 proteome (2019-nCoV HKU-SZ-005b7). Search parameters specified a parent MS tolerance of 15 ppm and an MS/MS fragment ion tolerance of 0.4 Da, with up to two missed cleavages allowed for trypsin/Lys-C. Deamidation (NQ), oxidation (M), acetylation (protein N-term), NEM (C), and palmitoylation (C) were set as variable modifications. Search results were processed using the trans-proteomic pipeline (version 4.7), and proteins with an iProphet probability ≥0.9 with at least two unique peptides matched were considered high-confidence identifications. Bayesian statistics (SAINT) (34) were applied to compare NaCl-treated samples to hydroxylamine-treated samples in order to identify putative acylated proteins. Control (NaCl-treated) and hydroxylamine-treated replicates were compressed to 2, and a Bayesian false discovery rate cutoff of 1% was used.

## RESULTS

### SARS-CoV-2 spike protein is S-acylated

Alignment of the C-terminal cytoplasmic tails of several human and murine CoVs reveals that the 20 amino acids adjacent to the membrane are highly enriched in Cys residues (Fig. 1A). Indeed, in the case of SARS-CoV-2 spike, half of the first 20 amino acids are Cys residues, providing ample sites for potential S-acylation. To explore this possibility, we first established a model to express and study the SARS-CoV-2 spike protein using ectopic expression of spike tagged at the C-terminus with a C9 epitope (TETSQVAPA) (supplemental Fig. S1) (35, 36). Immunoblotting of the Spike-C9 revealed numerous reactive bands in transfected cells but none in controls (Fig. 1B, C). Consistent with previous reports (36, 37), we detected two spike molecular species, a full-length ~190 kDa and a ~100 kDa fragment compatible with the furin-cleaved S2 fragment. To determine if the ectopically expressed Spike-C9 protein is acylated, we incubated transfected cells with BSA-conjugated alkynyl-palmitate (15-hexadecynoic acid; 15-HDYA), a “clickable” palmitate analog (38). Spike-C9 immunocaptured using anti-C9 beads was reacted with Cy5.5-azide using a copper(I)-catalyzed azide-alkyne cycloaddition (39–41). As shown in Fig. 1D, the Spike-C9 from cells incubated with alkynyl-palmitate and reacted with the Cy5.5-azide generated a similar banding pattern as the anti-C9 antibody, indicating that the full-length and S2 fragment of the spike protein are both acylated.

Considering that the SARS-CoV-2 spike protein cytoplasmic tail contains 10 Cys residues, we sought to confirm that the modifications are on Cys residues and examine the extent of modification. To do this, we used an approach termed acyl-polyethylene glycol (PEG) exchange (APE) that involves substituting acyl groups attached to Cys residues with a 5 kDa PEG mass tag (42).

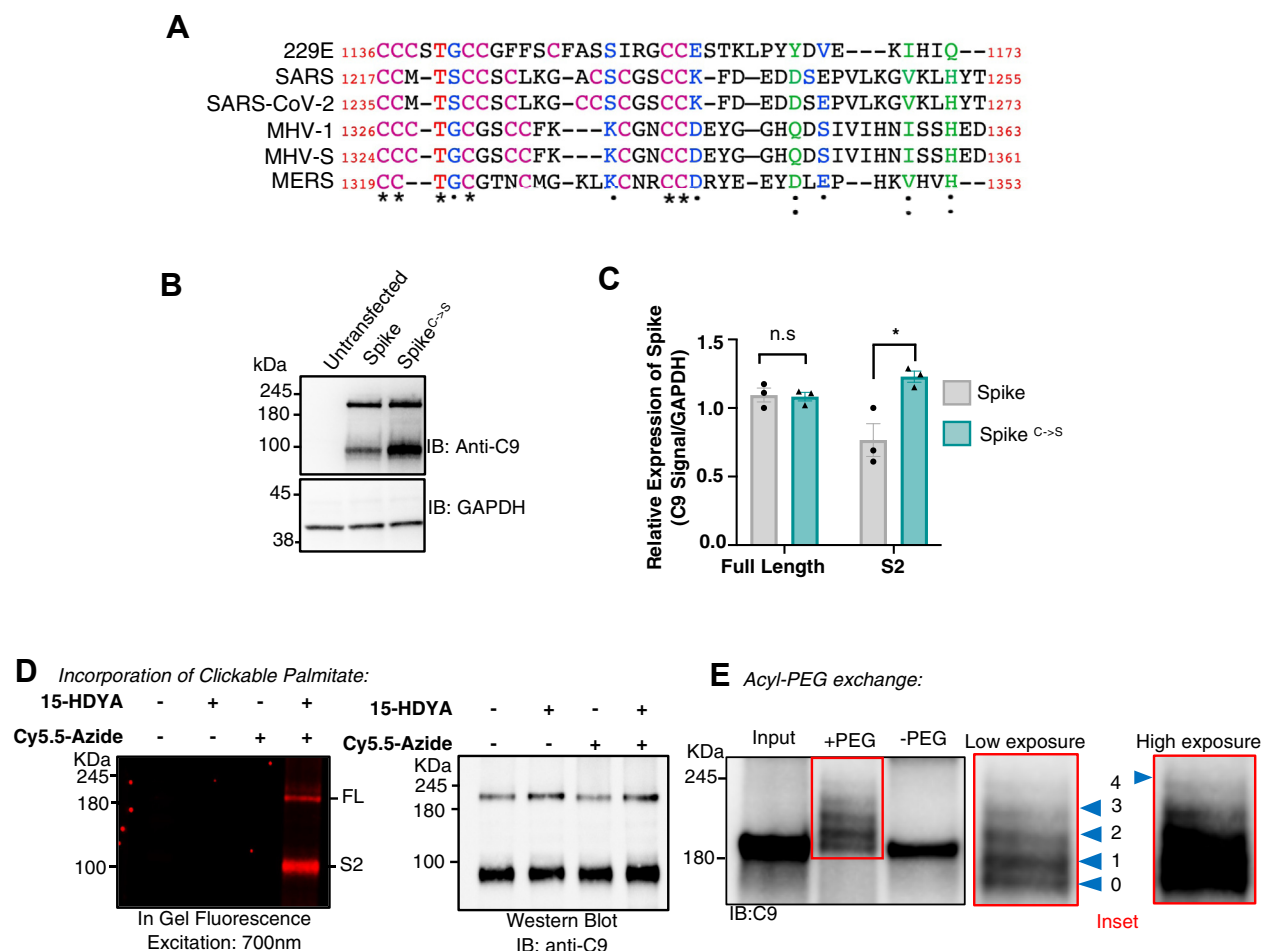


**Fig. 1.** S-acylation of the SARS-CoV-2 spike protein. **A:** Sequence alignment of the cytosolic amino acids adjacent to the transmembrane domain of murine and human coronavirus spike proteins. Adapted from ClustalW; (\*) residue is wholly conserved, (:) strongly similar properties, (.) weakly similar properties conserved. **B:** Immunoblots of ectopically expressed Spike-C9 and Spike<sup>C→S</sup>-C9 and GAPDH from total cell lysates of HEK293T cells. Cells were transiently transfected for 18 h prior to collection and subsequent immunoblotting with the anti-C9 antibody. Untransfected cells display no anti-C9 reactive bands, whereas cells transfected with Spike-C9 or the all Cys-to-Ser mutants have bands equivalent to the full-length protein and a cleaved S2 fragment. **C:** Quantitation of **B**. Data are means  $\pm$  SEM of  $n = 3$  biological replicates. Unpaired  $t$ -test with Welch's corrections, ns = not significant,  $P = 0.85$  and  $*P = 0.02$ . **D:** Incorporation of 15-HDYA ( $\omega$ -terminal alkyne containing palmitate analog) on Spike-C9 measured through click chemistry. The covalent addition of 15-HDYA to the Spike-C9 is determined following immunocapture using anti-C9 beads and a copper-catalyzed cycloaddition between the alkyne group Cy5.5-conjugated azide. Samples were resolved using gel electrophoresis and imaged using an LI-COR Odyssey (depicted as in-gel fluorescence and the left). Subsequently, samples were transferred to PVDF membrane for immunoblotting with an anti-C9 antibody followed by an HRP-conjugated secondary antibody and chemiluminescence (Western blot on the right). Omission of either the 15-HDYA or the Cy5.5-azide results in loss of specific fluorescence.  $N = 3$  biological replicates. **E:** Examination of the number of putative S-acylation sites. Lysates of HEK293T cells expressing the Spike-C9 epitope were subjected to the acyl-PEG exchange assay. Spike-C9 was immunocaptured using anti-C9 beads followed by the blocking of free thiol groups, cleavage of the thioester bond with hydroxylamine, and the covalent addition of the 5 kDa PEG to the freshly liberated thiol residues. Following the acyl-PEG assay, samples were resolved by electrophoresis and transferred to membranes for blocking and detection. Input: unprocessed HEK293T lysate, +PEG: deacylated and PEG covalent addition, and -PEG: deacylated without PEG addition. The inset of the acyl-PEG assay immunoblot (on the right) at low and high exposures demonstrates an unmodified protein and four addition bands indicating that a reaction of the spike has at least four sites of S-acylation,  $n = 3$  biological replicates.

The unreacted protein (input) and the protein treated with hydroxylamine, to cleave the thioester bond and remove the fatty acyl chains, but not reacted with PEG (-PEG), have an apparent molecular weight of  $\sim 190$  kDa (Fig. 1E). Spike-C9 treated with hydroxylamine and reacted with a maleimide-functionalized 5 kDa PEG revealed five distinct bands consistent with an unmodified band and four sites of S-acylation.

Given the proximity of the 10 Cys residues within a 20 amino acid stretch, it is unclear if the addition of multiple 5 kDa PEG molecules could be sterically hindered. Another possibility is that the addition of the C9 epitope to the C-terminal end of the spike may result in less or variable acylation. Regardless, these results suggest that the spike protein can be modified on numerous Cys residues and that some of the individual



proteins are modified with a minimum of four acyl chains.

Next, we sought to confirm the results obtained using the heterologously expressed epitope-tagged spike with the native spike in cells infected with the SARS-CoV-2. We used a strategy termed acyl-RAC (43). In this workflow, free Cys residues are chemically blocked using NEM. Next acyl-Cys thioester linkages are then cleaved using hydroxylamine, and then treated lysates are incubated with thiol-reactive beads allowing for the capture of the previously S-acylated proteins by a mixed disulphide exchange reaction. This assay is readily coupled to MS-based protein detection and quantitation. As shown in Tables 1, S1, and S2, the acyl-RAC MS workflow can identify numerous host proteins that are known to be S-acylated, including flotillin, calnexin, scribble, and SNAP23 in both Vero and HEK293 stably expressing both the ACE2 receptor and TMPRSS2 protease (or simply HEK A2T2) (44). Analysis of cells infected with SARS-CoV-2 revealed the presence of the spike protein that was one of the most abundant S-acylated proteins in both cell types. Furthermore, despite the infection, most of the other host S-acylated proteins were unaltered. These results collectively suggest that both the ectopically expressed spike and native spike delivered during SARS-CoV-2 infection are S-acylated.

### S-acylation of SARS-CoV-2 spike protein is required for membrane fusion

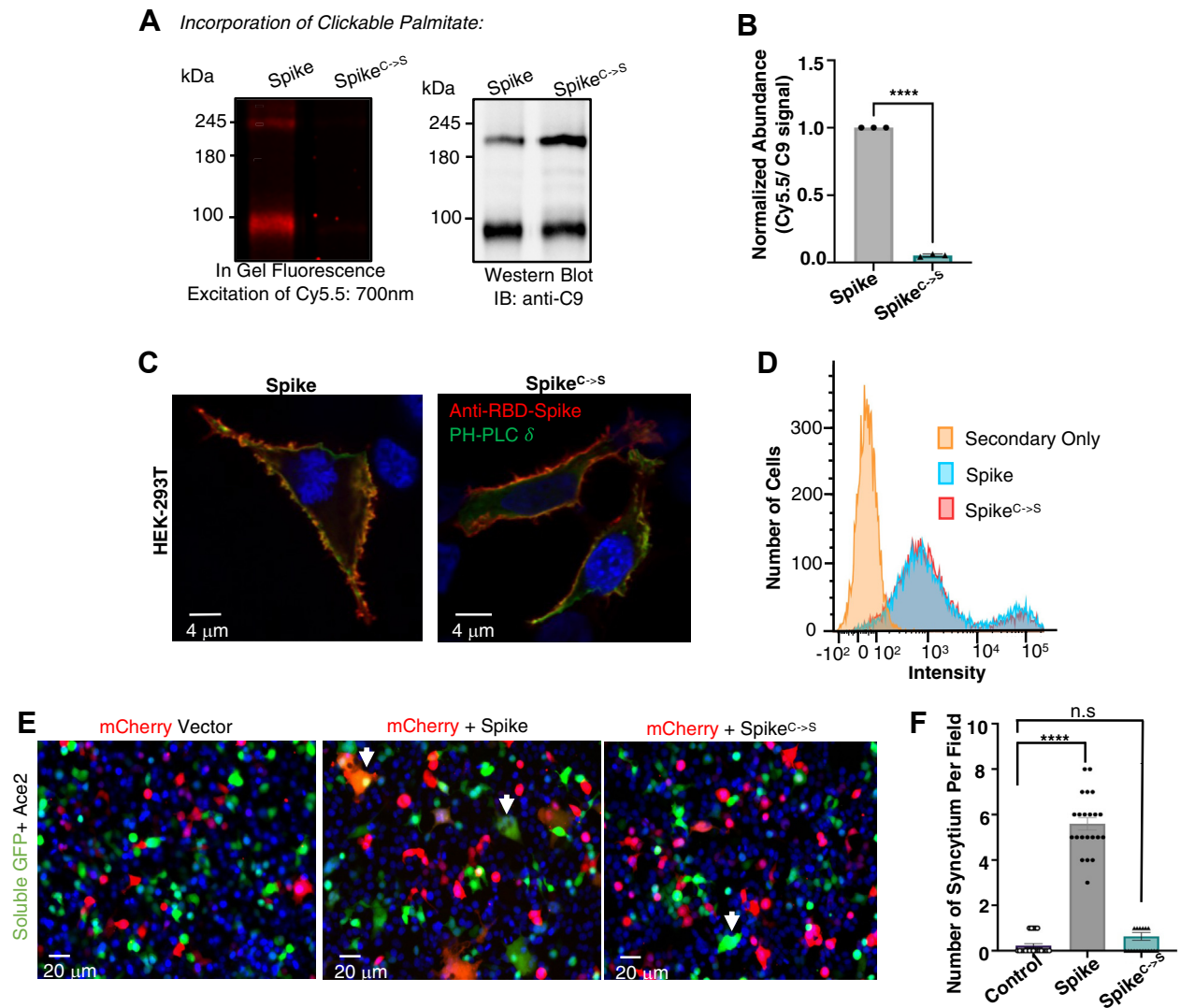
The CoV spike polypeptides are class I viral fusion proteins that mediate membrane fusion (45). This function is essential to initiating viral infection. To investigate the role of S-acylation of the SARS-CoV-2 spike protein in this process, we used a site-directed mutagenesis approach to mutate all 10 Cys residues in the cytoplasmic tail to Ser (termed Spike<sup>C>S</sup>) (supplemental Fig. S1). Lysates of HEK293T cells ectopically expressing Spike-C9 and Spike<sup>C>S</sup>-C9 were immunoblotted and revealed that the full-length Spike<sup>C>S</sup>-C9 was expressed at comparable levels to the wild-type protein and that there is also the production of the S2 fragment (Fig. 1A, B). During our studies, we noticed that the relative proportion of full-length compared with the S2 was variable but consistent within individual biological replicates. Whether this is due to a cell-autonomous factor, the efficiency of transfection, or perhaps even after cell lysis, proteolysis was not determined. We next confirmed that the Spike<sup>C>S</sup>-C9 fails to incorporate 15-HDYA, suggesting it is not S-acylated (Fig. 2A, B). Recent studies have demonstrated that the C-terminal region of spike interacts with a variety of vesicular transport machinery, including the COPI and COPII coatomers (46). To determine if loss of the S-acylation sites alters the protein delivery to the plasma membrane, we used an antibody that detects an extracellular epitope together with immunofluorescence microscopy and flow

TABLE 1. Twenty most abundant S-acylated proteins in SARS-CoV2 infected cells

Gene symbol	Gene name
Vero cells	
<i>Spike</i>	SARS-CoV-2 Spike protein
<i>FASN</i>	Fatty acid synthase
<i>FLOT2</i>	Flotillin 2
<i>FLOT1</i>	Flotillin 1
<i>TXNRD1</i>	Thioredoxin reductase 1
<i>MYOF</i>	Myoferlin
<i>CANX</i>	Calnexin
<i>MTDH</i>	Metadherin
<i>UBE2L3</i>	Ubiquitin conjugating enzyme E2 L3
<i>RHBDD2</i>	Rhomboid domain containing 2
<i>LSR</i>	Lipolysis stimulated lipoprotein receptor
<i>DLAT</i>	Dihydrolipoamide S-acetyltransferase
<i>STOM</i>	Stomatin
<i>SCRIB</i>	Scribble planar cell polarity protein
<i>SNAP23</i>	Synaptosome associated protein 23
<i>CKAP4</i>	Cytoskeleton associated protein 4
<i>ALDH2</i>	Aldehyde dehydrogenase 2 family member
<i>ABCC4</i>	ATP binding cassette subfamily C member 4
<i>CD151</i>	CD151 molecule (Raph blood group)
<i>CLDN1</i>	Claudin 1
HEK A2T2 cells	
<i>Spike</i>	SARS-CoV-2 Spike protein
<i>FASN</i>	Fatty acid synthase
<i>CANX</i>	Calnexin
<i>UBE2L3</i>	Ubiquitin conjugating enzyme E2 L3
<i>FLOT1</i>	Flotillin 1
<i>FLOT2</i>	Flotillin 2
<i>IRS4</i>	Insulin receptor substrate 4
<i>CKAP4</i>	Cytoskeleton associated protein 4
<i>MTDH</i>	Metadherin
<i>ACAT1</i>	Acetyl-CoA acetyltransferase 1
<i>SCAMP3</i>	Secretory carrier membrane protein 3
<i>ACAT2</i>	Acetyl-CoA acetyltransferase 2
<i>DLAT</i>	Dihydrolipoamide S-acetyltransferase
<i>SLC1A5</i>	Solute carrier family 1 member 5
<i>SCRIB</i>	Scribble planar cell polarity protein
<i>AUP1</i>	AUP1 lipid droplet regulating VLDL assembly factor
<i>SNAP23</i>	Synaptosome associated protein 23
<i>RHBDD2</i>	Rhomboid domain containing 2
<i>CYB5B</i>	Cytochrome b5 type B
<i>ATP2A2</i>	ATPase endoplasmic reticulum Ca2+ transporting 2

cytometry. We confirmed that comparable amounts of both the Spike-C9 and Spike<sup>C>S</sup>-C9 traffic to the plasma membrane (Fig. 2C, D). Together, these results demonstrate that mutagenesis of the cytoplasmic Cys residues to Ser and the concomitant loss of S-acylation have minimal impact on expression levels and transport to the cell surface.

Previous studies have demonstrated that the SARS-CoV-2 spike protein can catalyze syncytium formation, provided that neighboring cells express ACE2 (6). To determine if S-acylation of the spike protein is required for syncytium formation, we utilized a coculture strategy where cells cotransfected with plasmids encoding Spike-C9 and soluble mCherry were cocultured with cells cotransfected with plasmids encoding ACE2 and soluble GFP. Cocultures containing cells expressing mCherry alone and cells with ACE2/GFP showed no signs of cell-cell fusion, as expected (Fig. 2E, F). However, cocultures with Spike/mCherry and ACE2/GFP displayed numerous large syncytia-containing soluble GFP and mCherry (Fig. 2E, F). In



**Fig. 2.** S-acylation of the SARS-CoV-2 spike protein is required for cell-cell fusion (A). Clickable palmitate is not covalently attached to Spike<sup>C->S</sup>. Cells expressing either Spike-C9 or Spike<sup>C->S</sup>-C9 were incubated with 15-HDYA and subsequently processed using copper-catalyzed cycloaddition of Cy5.5-azide as for Figure 1B. The degree of protein lipidation was detected by in-gel fluorescence of Cy5.5-azide (exposed at 700 nm; left of the image); corresponding protein levels were detected by chemiluminescence (right of the image). B: Quantitation of A and the labeling by exogenously added 15-HYDA. The abundance is presented as the quotient of the intensities of the Cy5.5 signal from the attached fatty acid and the C9 epitope detected by immunoblotting. Data are means  $\pm$  SEM of  $n = 3$  biological replicates and analyzed using an unpaired  $t$ -test with Welch's correction; \*\*\*\* $P < 0.0001$ . C: Confocal imaging of surface-exposed and immunostained Spike and Spike<sup>C->S</sup>. Immunofluorescence of Spike-C9 and Spike<sup>C->S</sup>-C9 ectopically expressed and stained with an anti-receptor binding domain (RBD) of spike antibody (red) in nonpermeabilized HEK293T cells. Cells were cotransfected with the pleckstrin homology domain of phospholipase C8 (GFP-PH-PLC $\delta$ ), which delineated the plasma membrane,  $n = 3$  biological replicates. D: flow cytometry of surface-exposed spike and the S-acylation deficient mutant as in C,  $n = 3$  biological replicates. E: Micrographs of mCherry and GFP-expressing coculture to assess syncytium formation. HEK293T cells expressing mCherry and empty vector, Spike-C9, or Spike<sup>C->S</sup>-C9 were plated with HEK293T cells expressing soluble GFP and the ACE2 receptor. Representative two-color merged micrographs demonstrate that wild-type spike and ACE2 coculture form syncytium (Orange) indicated with white arrows. F: Quantitation of E, the number of syncytia per microscope field of view was counted, and 10 microscope fields of each condition per experiment were analyzed. Data are means  $\pm$  SEM of  $n = 3$  biological replicates and analyzed by one-way ANOVA; \*\*\*\* $P < 0.0001$ , ns,  $P = 0.2418$  compared with control.

contrast, HEK293T cells expressing Spike<sup>C->S</sup>-C9/mCherry cocultured with ACE2/GFP-expressing cells displayed only a few smaller mCherry and GFP double-positive cells (Fig. 2E, F). These results suggest that one or more membrane proximal cytoplasmic Cys residues are required for the spike protein to facilitate syncytium formation in this in vitro assay.

### ZDHHC5 is required for human CoV infection

The human genome encodes a family of 24 ZDHHC (including ZDHHC11B) palmitoyltransferases (22). ZHHC5 was reported to interact with the SARS-CoV-2 spike protein physically, as shown using immunoprecipitation-MS (13). We confirmed these results using coimmunoprecipitation and found that



Spike-C9 could transiently interact with HA-tagged ZDHHC5 (supplemental Fig. S2). Given that numerous ZDHHC enzymes have been demonstrated to S-acylate the spike protein, we wanted to determine the relative importance of ZDHHC5. Thus, we assessed the contribution of ZDHHC5 to the S-acylation of spike in parental HEK293T cells and genome-edited cells deficient in ZDHHC5 expression (supplemental Fig. S3). Spike-C9 was transiently expressed in wild-type and ZDHHC5<sup>K/O</sup> cells, incubated with 15-HDYA and subsequently processed as in Fig. 1 to determine the extent of S-palmitoylation. Notably, the loss of ZDHHC5 resulted in nearly a 40% reduction in Spike S-palmitoylation (Fig. 3A, B). Thus, even though reports demonstrate that upward of 11 ZDHHC enzymes can modify spike, our experiments with the clickable palmitate suggest ZDHHC5 is responsible for a significant fraction of the post-translational modification.

As mentioned previously, the 15-HDYA experiment does not provide information about the number of sites being modified. Furthermore, 15-HDYA does not provide information on whether other fatty acids can be attached to the spike protein. We sought to investigate the extent of S-acylation using complementary approaches. First, cells ectopically expressing Spike-C9 and 3×HA-ZDHHC5 were processed using the APE assay as in Fig. 1E. The increased expression of ZDHHC5 resulted in a ~3-fold increase in S-acylation as detected by APE, along with the appearance of a sixth band at a higher molecular weight (Fig. 3C, D). Unlike the metabolic labeling with clickable fatty acids, the APE assay detects sites of S-acylation regardless of the source of the acyl chains. Next, we considered whether the spike protein was modified by acyl chains other than palmitate and whether overexpression of the ZDHHC5 enhanced this modification. To investigate this possibility, cells were metabolically labeled with BSA-conjugated clickable fatty acid analogs of palmitate, stearate, and myristate, followed by immunocapture and processing as in Fig. 1D. As depicted in Fig. 3E, F, the myristate analog (13-TDYA) and stearate analog (17-ODYA) are covalently attached to the Spike-C9 but less abundant. Curiously, we also found that overexpression of ZDHHC5 had a modest impact on the labeling of spike by 15-HDYA compared with control cells (supplemental Fig. S4). We hypothesize that this is because either the uptake from the medium or the synthesis of the 15-HDYA-CoA is a limiting step, and in the presence of de novo synthesized palmitoyl-CoA, it is inefficiently used to S-acylate proteins. Indeed when we repeat the experiment in the presence of the FASN inhibitor TVB-3166, we see more efficient incorporation of the clickable label (supplemental Fig. S4).

As part of the reaction cycle, ZDHHC enzymes are first autoacylated with the acyl chains and subsequently transferred to the substrates (47). To our knowledge, no information is available on the fatty acyl specificity of ZDHHC5. Thus, taking advantage of the clickable fatty

acids and protocol used in Fig. 3E, we sought to determine which fatty acids are attached to ZDHHC5 as part of the reaction cycle. As shown in Fig. 3G, H, ZDHHC5 displays a strong preference for 16-carbon acyl chains even compared with the 14- and 18-carbon chains. The results suggest that ZDHHC5 is responsible for a substantial amount of the palmitate attached to the spike protein, but that other ZDHHC enzymes attach other fatty acyl chains to the spike protein.

### ZDHHC5 supports human CoV-229E Spike S-acylation and infection

Next, we sought to investigate if our observations on the spike protein and ZDHHC5 can be extended to another human CoV, namely CoV-229E, one of the viruses that cause the common cold. Although the spike protein of CoV-229E recognizes a different host protein, CD13 (48), its cytosolic tail is similar to that of SARS-CoV-2 (Fig. 1A). We again generated a plasmid-borne C9-tagged spike protein of the 229E virus (229E Spike-C9). Using the APE assay, we found that the 229E Spike-C9 protein is S-acylated on multiple sites when ectopically expressed in HEK293T cells. Curiously, the pattern obtained was different from that of the SARS-CoV-2 spike. First, we found that all the 229E Spike-C9 had at least one PEG attached (Fig. 4A) and that we could not resolve the individual bands. This raises the possibility that the 229E spike is more heavily S-acylated than the SARS-CoV-2 spike. Again, the intensity of the PEGylated proteins is enhanced when HA-ZDHHC5 levels are increased (Fig. 4A, B). This finding is consistent with the spike proteins of SARS-CoV-2 and likely 229E being a substrate of ZDHHC5. To our knowledge, the role of other ZDHHC enzymes and the 229E spike has not been investigated, and our results do not rule out the possibility that other ZDHHC enzymes may also modify the 229E spike protein.

To investigate the role of ZDHHC5 in the generation of virulent progeny, we used two complementary cell-based assays. First, we used a previously described siRNA to silence *ZDHHC5* in confluent monolayers of human MRC-5 fibroblasts (Fig. 4C, D) (27). Next, we used these conditions and assessed the ability of CoV-229E to form plaques (Figs. 4E, F and S5A). Cell monolayers transfected with a nontargeting siControl produced an average of ~10<sup>6</sup> plaque-forming unit/ml, and monolayers transfected with the siZDHHC5 displayed significantly fewer plaques. From the plaque assay, it was unclear if the loss of ZDHHC5 impacted the initial infection or the subsequent spread to the neighboring cells in the monolayer. Thus, we used a liquid culture assay to complement the plaque assay to investigate infection and dissemination. In this assay, cells were incubated in the presence of 229E virus at a low MOI (MOI = 0.005) for 2 h, followed by extensive washing. After 72 h, cells were processed and stained with an antibody directed against the 229E spike protein (24) and an Alexa Fluor 488-conjugated secondary

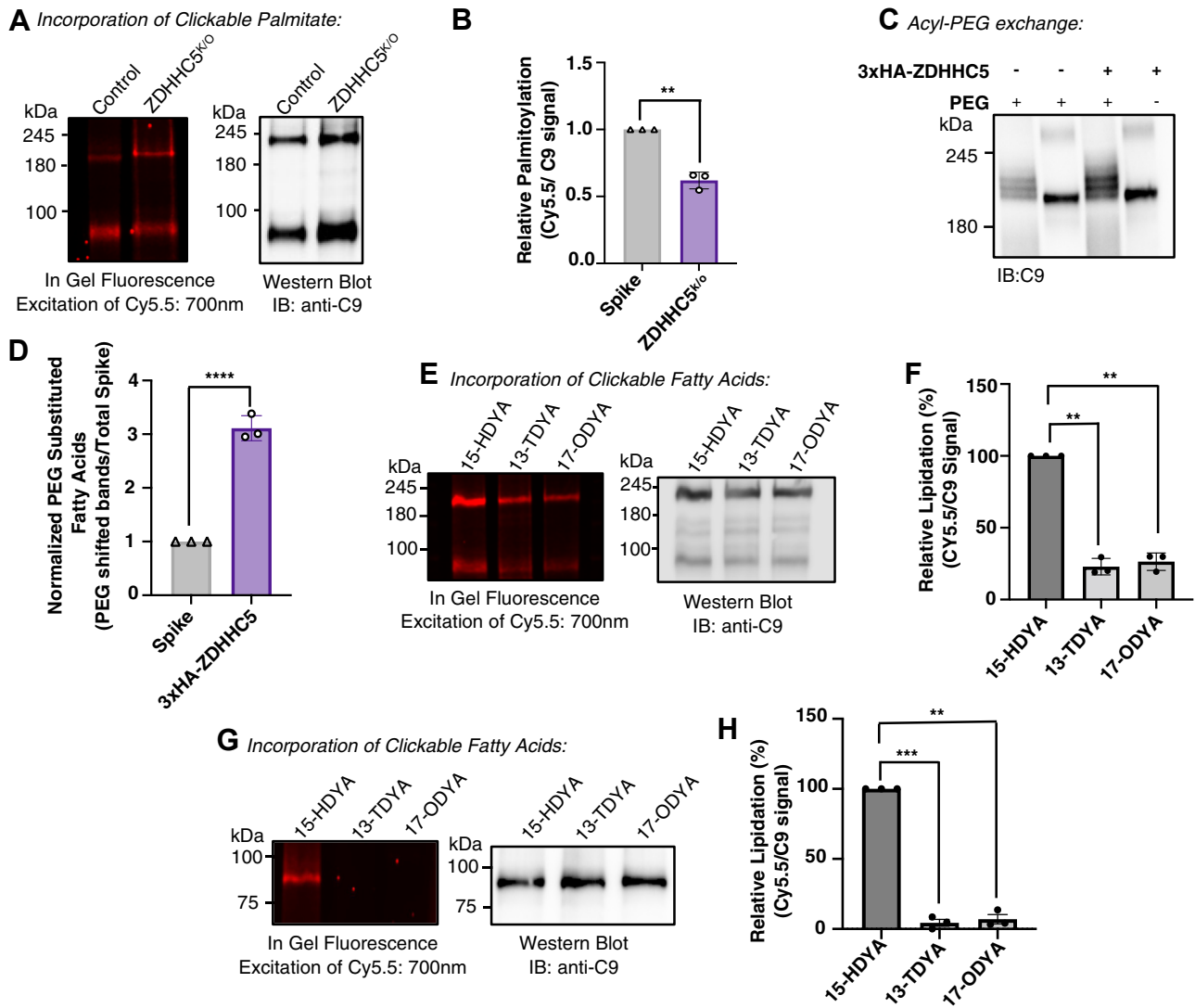


**Fig. 3.** The acyltransferase ZDHHC5 contributes to the S-acylation of spike with a preference for palmitate. A: Control and genome-edited *ZDHHC5* knockout HEK293T cells were incubated with 15-HDYA and processed using a click chemistry reaction (Figure 1D). Covalent attachment of the clickable palmitate analog was determined by Cy5.5 in-gel fluorescence (exposure 700 nm; left of the image), with the corresponding protein levels determined following transfer to membrane and immunoblotting using chemiluminescence (right of the image). B: Quantitation of A. Relative palmitoylation levels were calculated as the quotient of the Cy5.5 signal and the C9 chemiluminescence. Data are the means  $\pm$  SEM of  $n = 3$  biological replicates and analyzed using an unpaired  $t$ -test with Welch's correction;  $**P = 0.0089$ . C: Control cells and cells transiently transfected with 3xHA-ZDHHC5 were processed using the acyl-PEG exchange assay as for Figure 1E. Following the 5-kDa PEG substitution, samples were resolved, transferred, and immunoblotted using the anti-C9 antibody. D: Quantitation of C, whereby the shifted PEGylated bands of the 180 kDa spike are normalized to the unmodified band at  $\sim 180$  kDa; this band migrated to the same position as the minus PEG sample. In individual experiments, the value of the control cells was set equal to 1, and the relative intensity of the ZDHHC5 overexpressing cells was determined as a relative measurement. Data are the mean  $\pm$  SEM of  $n = 3$  biological replicates and analyzed with an unpaired  $t$ -test with Welch's correction;  $***P < 0.0001$  compared with controls. E: Cells coexpressing Spike-C9 and 3xHA-ZDHHC5 were incubated with alkyne-containing clickable analogs of myristate (13-TDYA) and palmitate (15-HDYA) and stearate (17-ODYA) for 2 h. The spike protein was immunocaptured and processed as for Figure 1B. In-gel fluorescence of the Cy5.5 (left) and immunoblots of the anti-C9 (right) are shown. F: Relative lipidation of Spike-C9, whereby the Cy5.5-azide in-gel fluorescence was normalized to the total Spike-C9 protein levels measured by chemiluminescence. Data are the mean  $\pm$  SEM of  $n = 3$  individual trial replicates analyzed by multiple  $t$ -tests with Welch's correction;  $**P < 0.001$  compared with 15-HDYA. G: Cells ectopically expressing 3xHA-ZDHHC5 were incubated with clickable fatty acids as in E. Immunocapture using an anti-HA antibody and Protein A beads were used to purify 3xHA-ZDHHC5 from lysates and subjected to click chemistry analysis as in E. The results demonstrate that ZDHHC5 does not readily autoacyl using CoA derivatives of the clickable myristate and stearate. H: Relative lipidation of 3xHA-ZDHHC5, whereby the Cy5.5-azide in-gel fluorescence was normalized to the total 3xHA-ZDHHC5 protein levels measured by chemiluminescence. Data are the mean  $\pm$  SEM of  $n = 3$  individual trial replicates analyzed by multiple  $t$ -tests with Welch's correction;  $***P = 0.0007$ ,  $**P < 0.001$  compared with 15-HDYA.

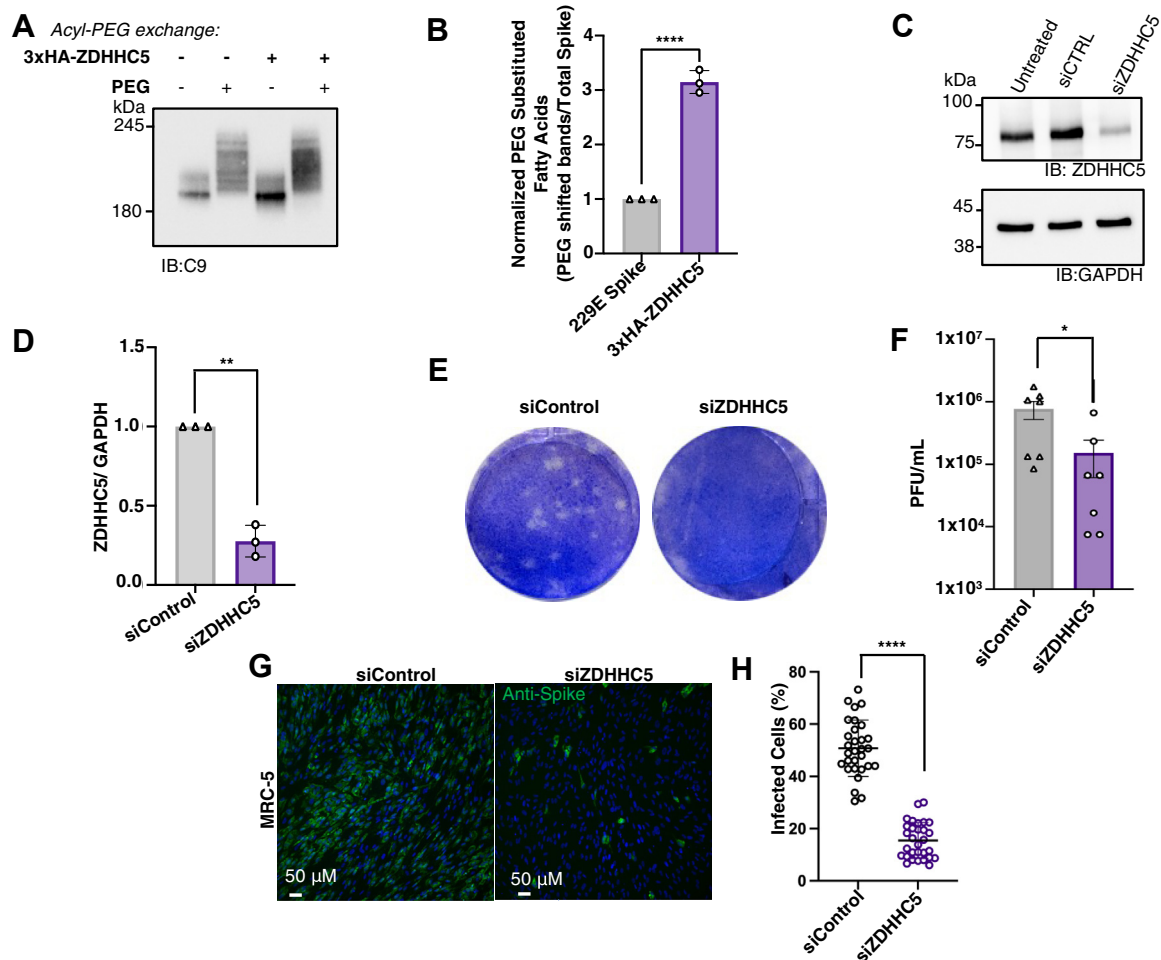


**Fig. 4.** Increased expression of *ZDHHC5* increases S-acylation of human CoV 229E spike and is required for virulence. **A:** Acyl-PEG assay as for [Figure 1E](#) to examine the S-acylation of the 229E Spike-C9 in HEK293T cells transiently transfected with either the 3xHA-ZDHHC5 or empty vector. **B:** Quantitation of the acyl-PEG assay in **A**, where the higher molecular weight PEG-modified bands were normalized to the fastest migrating band. All bands in the +PEG sample migrated more slowly than the -PEG sample suggesting the 229E spike is more readily and perhaps more highly S-acylated. Data are the mean  $\pm$  SEM of  $n = 3$  biological replicates, unpaired  $t$ -test with Welch's correction, \*\*\*\* $P < 0.0001$ . **C:** MRC-5 cells were transfected with siRNA-control or siRNA-ZDHHC5, and lysates were collected and immunoblotted to examine the relative expression of ZDHHC5. **D:** Quantification of **C**. Data are the mean  $\pm$  SEM,  $n = 3$  biological replicates normalized to GAPDH and analyzed using an unpaired  $t$ -test with Welch's correction, \*\* $P = 0.0063$ . **E:** Representative image of plaques observed in MRC-5 cells silenced for ZDHHC5 infected with 229E for 5 days. This image is also included for [supplemental Fig. S5A](#), which demonstrates plaque assays analyzed for this figure. **F:** Quantification of 229E PFU/ml in MRC-5 cells silenced for ZDHHC5 as shown in **E**, unpaired  $t$ -test, \* $P = 0.0371$ . Data are mean  $\pm$  SEM of  $n = 3$  biological replicates. **G:** Representative images of MRC-5 cells silenced for ZDHHC5 and infected with 229E at an MOI of 0.0005. Images labeled as follows: spike 229E (green), DAPI (blue). **H:** Quantification of 229E infection assay where each data point represents a 10 $\times$  magnified field of view, where an average of 600 cells was counted in ImageJ, 10 fields of view per condition for  $n = 3$  biological replicates were analyzed; unpaired  $t$ -test, \*\*\*\* $P < 0.0001$ . Data are mean  $\pm$  SEM.

antibody. As shown in [Fig. 4G, H](#),  $\approx 50\%$  of the siControl cells were infected as determined by immunofluorescence detection of the spike protein. In contrast, only  $\approx 15\%$  of the ZDHHC5-silenced cells were positive for the spike protein. These results are consistent with the notion that ZDHHC5 is required for the generation of virulent progeny and spread in vitro.

#### De novo fatty acid synthesis is required for CoV infectivity

Based on our data, we sought to determine if ZDHHC5 and other ZDHHC enzymes could represent

suitable therapeutic targets for treating CoV infections. Unfortunately, no specific inhibitor of ZDHHC5 exists. Previously, we found that the FASN inhibitor cerulenin prevented the S-palmitoylation of the ZDHHC5 substrates NOD1 and NOD2 ([25](#)). This is logical since FASN produces a cytosolic pool of palmitoyl-CoA, the palmitate donor for ZDHHCs. However, cerulenin is not suitable therapeutically because of severe weight loss and off-target effects in murine models ([49–51](#)). Fortunately, first-in-class FASN inhibitors have been developed by Sagimet Biosciences (San Mateo, CA). One of these inhibitors,



TVB-2640, is orally available, well tolerated, and a highly potent FASN inhibitor in clinical trials for cancer (52) and nonalcoholic fatty liver disease (53). A commercially available related compound, TVB-3166, previously showed an  $IC_{50}$  in vitro of 42 nM with a cellular  $IC_{50}$  of 60 nM (54, 55).

Since we wanted to achieve complete inhibition of FASN, we used higher concentrations of TVB-3166. Treating cells with 0.2  $\mu$ M or 20  $\mu$ M TVB-3166 did

neither impact cell viability nor alter the expression of Spike-C9 in HEK293T cells (Fig. 5A, B). However, treating HEK293T cells expressing Spike-C9 with TVB-3166 or 2-bromopalmitate, a nonspecific inhibitor of ZDHHC enzymes and other enzymes involved in fatty acid metabolism (56), attenuated the S-acylation of the spike protein as determined by the APE assay (Fig. 5C, D). In addition, we examined whether TVB-3166 directly inhibits ZDHHC5 by assessing the covalent

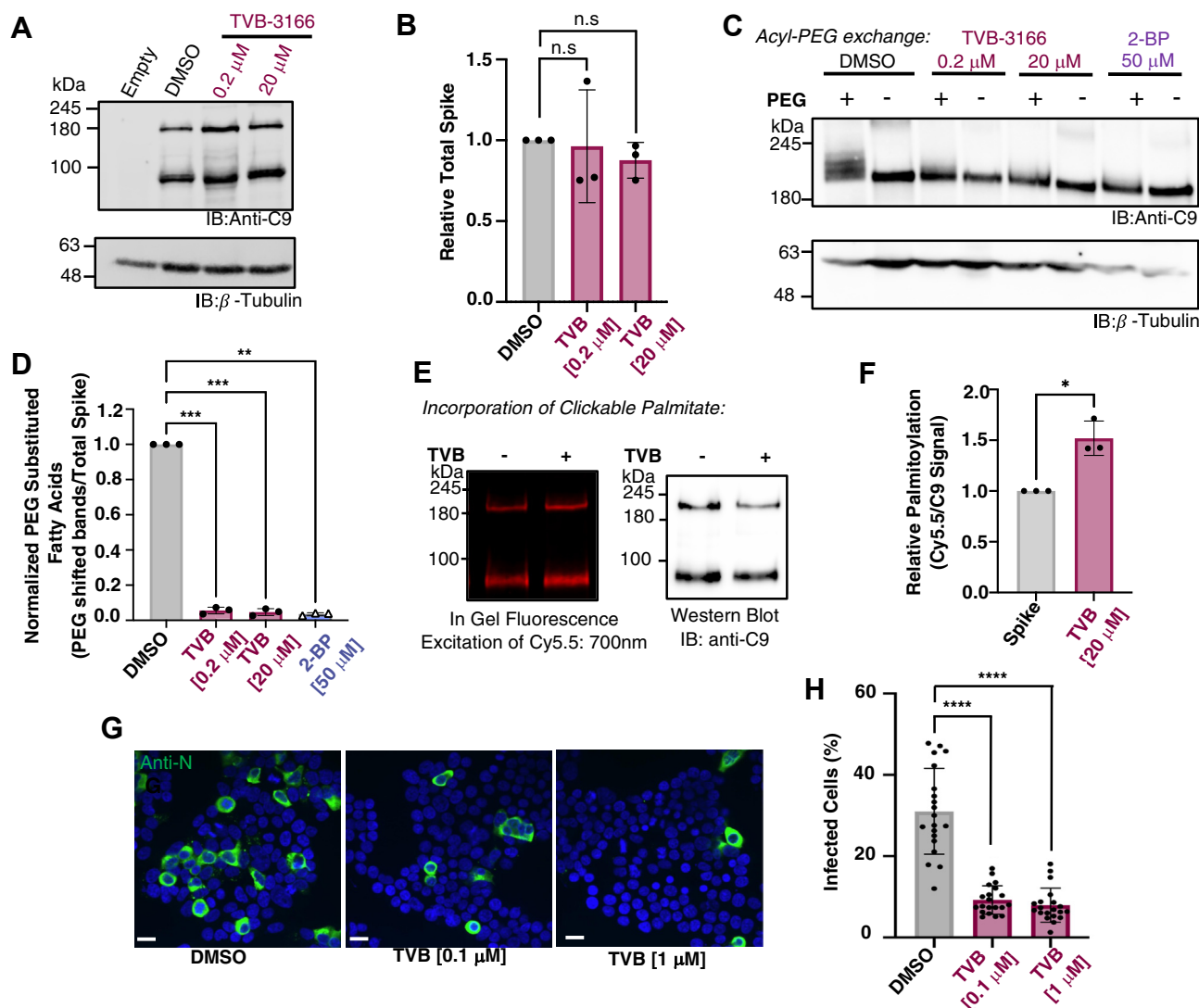


**Fig. 5.** Inhibition of FAS abolishes S-acylation of spike and attenuates SARS-CoV-2 spread in vitro. **A:** Immunoblot of ectopically expressed Spike-C9 in HEK293T cells treated with DMSO, 0.2  $\mu$ M or 20  $\mu$ M TVB-3166 for 16–18 h. **B:** Quantification of **A**. Data are the mean  $\pm$  SEM,  $n = 3$  biological replicates normalized to GAPDH and analyzed using an unpaired  $t$ -test with Welch's correction: 0.2  $\mu$ M,  $P = 0.8637$  and 20  $\mu$ M,  $P = 0.1243$ . Inhibition of FASN does not grossly impact the stability of the spike protein. **C:** Acyl-PEG exchange assay of Spike-C9 ectopically expressed in HEK293T treated with 0.2  $\mu$ M or 20  $\mu$ M TVB-3166 or 50  $\mu$ M 2-bromohexadecanoic acid (2-BP) for 16–18 h. **D:** Quantification of **C**, where PEG-modified bands were divided by the unmodified bands at  $\sim$ 180 kDa, multiple unpaired  $t$ -tests with Welch's correction, \*\*\* $P = 0.0001$ , \*\* $P = 0.0088$  relative to DMSO control. Data are mean  $\pm$  SEM of  $n = 3$  biological replicates. **E:** In-gel fluorescence (left) and immunoblotting (right) of Spike-C9 incubated with 15-HDYA following the treatment of DMSO or 20  $\mu$ M TVB-3166 for 18 h. Samples are processed as for Figure 1D. **F:** Quantitation of **E**. Data are the mean  $\pm$  SEM,  $n = 3$  replicates and analyzed using an unpaired  $t$ -test with Welch's correction, \* $P = 0.0334$ . **G** and **H:** Representative images and quantification of HEK293T A2T2 cells (stably expressing Ace2 and TMPRSS2) infected with SARS-CoV-2 (strain SB3, MOI of 0.1), treated with either 0.1  $\mu$ M or 1  $\mu$ M TVB-3166 6 h postinfection and incubated an additional 18 h. Data are the mean  $\pm$  SEM from  $n = 3$  replicates with all microscope fields plotted as individual points. Data were analyzed using a one-way ANOVA, \*\*\*\* $P < 0.0001$  relative to DMSO. The scale bar represents 6  $\mu$ m.

attachment of 15-HDYA on the spike protein in the presence of TVB-3166. Consistent with [supplemental Fig. S4](#), we find that the exogenously added clickable fatty acid is incorporated more efficiently in the presence of the FASN inhibitor ([Fig. 5E, F](#)), suggesting that there is competition between the endogenous acyl-CoAs and exogenous acyl chains. Our results suggest that in HEK cells, palmitoyl-CoA generated by FASN is the preferred substrate of ZDHHC enzymes and that exogenously added fatty acids have less of a role. Considering 2-BP is an exogenously added fatty acid, our results bring into question the mode of action of 2-BP and whether it truly needs to be converted to 2-BP-CoA to inhibit ZDHHC enzymes. Indeed, a previous study demonstrated that both 2-BP and 2-BP-CoA could directly modify Cys residues of ZDHHC enzymes ([56](#)). Furthermore, 2-BP can directly modify Cys residues on target proteins. We did not determine if 2-BP was bound to the cytosolic tail of spike; however, the complexities of 2-BP in our experiment further highlight the need for selective and pan inhibitor of ZDHHC enzymes.

To evaluate the effect of TVB-3166 on the viral spread, HEK293 A2T2 cells were infected with SARS-CoV-2 strain SB3 ([30](#)) at an MOI of 0.1 and then treated with TVB-3166 6 h postinfection for an additional 18 h. Then, cells were fixed, permeabilized, stained for the SARS-CoV-2 nucleocapsid protein, and imaged with confocal microscopy. Notably, a ~70% decrease in infection was observed with TVB-3166 treatment ([Fig. 5G, H](#)). These experiments collectively suggest that inhibiting de novo lipid synthesis is an efficient way of attenuating S-acylation and that this strategy effectively blocks the spread of the SARS-CoV-2.

#### **TVB-3166-mediated inhibition of FASN attenuates human CoV-229E spread and extends the survival of mice infected with a murine CoV**

We confirmed that TVB-3166 treatment also inhibited the S-acylation of the 229E Spike-C9 protein. HEK293T cells were transiently transfected with 229E Spike-C9 and treated with TVB-3166; cell lysates were then subject to the ABE assay and revealed a decrease in the higher molecular weight species ([Fig. 6A, B](#)). We next measured the ability of 229E to form plaques following TVB-3166 treatment. As illustrated in [Fig. 6C, D](#), treatment with 0.2  $\mu$ M TVB-3166 attenuated the spread of 229E by  $\approx$ 85% ([supplemental Fig S5B](#)). Together, these results suggest that the TVB-3166 FASN inhibitor blocks CoV infection at least in part by attenuating spike S-acylation.

The cellular results demonstrating that TVB-3166 attenuated spike S-acylation and limited spread of the SARS-CoV-2 and 229E virus in cell-based assays motivated us to determine if this FASN inhibitor could be a useful prophylactic in a mouse model of a previously developed CoV respiratory infection using the MHV-S ([31](#)). For this, juvenile A/J mice were thus infected

intranasally with 150,000 tissue culture infectious dose 50% of MHV-S. This mode of infection results in a lung infection with pulmonary pathologies similar to SARS-CoV ([31](#)). In control mice, changes in health were noticed as early as 2 days postinfection; all proceeded to deteriorate as monitored by several health indicators, including decreased temperature, body weight, and activity ([Fig. 6E–G](#)). By day 5, all control mice were sacrificed as per animal care protocols. Previous experiments demonstrated that TVB-3166 is well tolerated by mice up to 100 mg/kg ([47](#)). As these are juvenile mice and the drug was delivered by oral gavage, we used a significantly lower dose of 30 mg/kg to limit the possibility of gastric reflux and inhalation of acid into the lungs. In addition, to help mitigate any potential metabolic deficiencies, we delivered the drug with a bolus of corn oil. In contrast to untreated mice, the animals treated daily with 30 mg/kg of TVB-3166 showed prolonged survival ([Fig. 6E](#)), with one animal recovering fully in this study. Thus, using a low dose of TVB-3166 at the time of infection, similar to a prophylaxis drug regimen, limited the progression of disease caused by MHV-S in vivo as marked by reduced clinical symptoms in treated mice. However, further studies are required to understand if the TVB compounds undergoing phase II clinical for other diseases ([57, 58](#)) could be a beneficial prophylactic for CoV exposure such as the murine CoV tested here.

## **DISCUSSION**

We and others have now established that the spike protein of SARS-CoV-2 is S-acylated. Here, we evaluate the S-acylation of the spike protein in three complementary approaches. First, by using acyl-RAC MS of Vero and ACE2 and TMPRSS2 expressing HEK cells infected with SARS-CoV-2. We show that the spike protein becomes one of the most abundant S-acylated proteins in host cells. Somewhat surprisingly, the viral infection does not have much impact on the abundance of other S-acylated host proteins, suggesting that infection itself does not result in a major subversion of the host ZDHHC enzymes. In addition to this acyl-RAC MS, we used the APE assay, which replaces endogenous fatty acids of S-acylated proteins with a PEG mass tag and found that at least four modified Cys residues in the spike protein ectopically expressed in HEK cells. Finally, we demonstrate that a variety of exogenously added clickable fatty acids, palmitate, myristate, and stearate, can be attached to the Cys residues of ectopically expressed spike protein. Together, these data demonstrate that the spike protein is S-acylated.

The S-acylation supports the ability of the spike protein to catalyze membrane fusion and thus the infectivity of the SARS-CoV-2 virus and pseudovirus models ([15, 18, 20](#)). Furthermore, these observations are similar to previous findings on MHV and SARS-CoV spike proteins ([21, 23](#)), demonstrating the importance

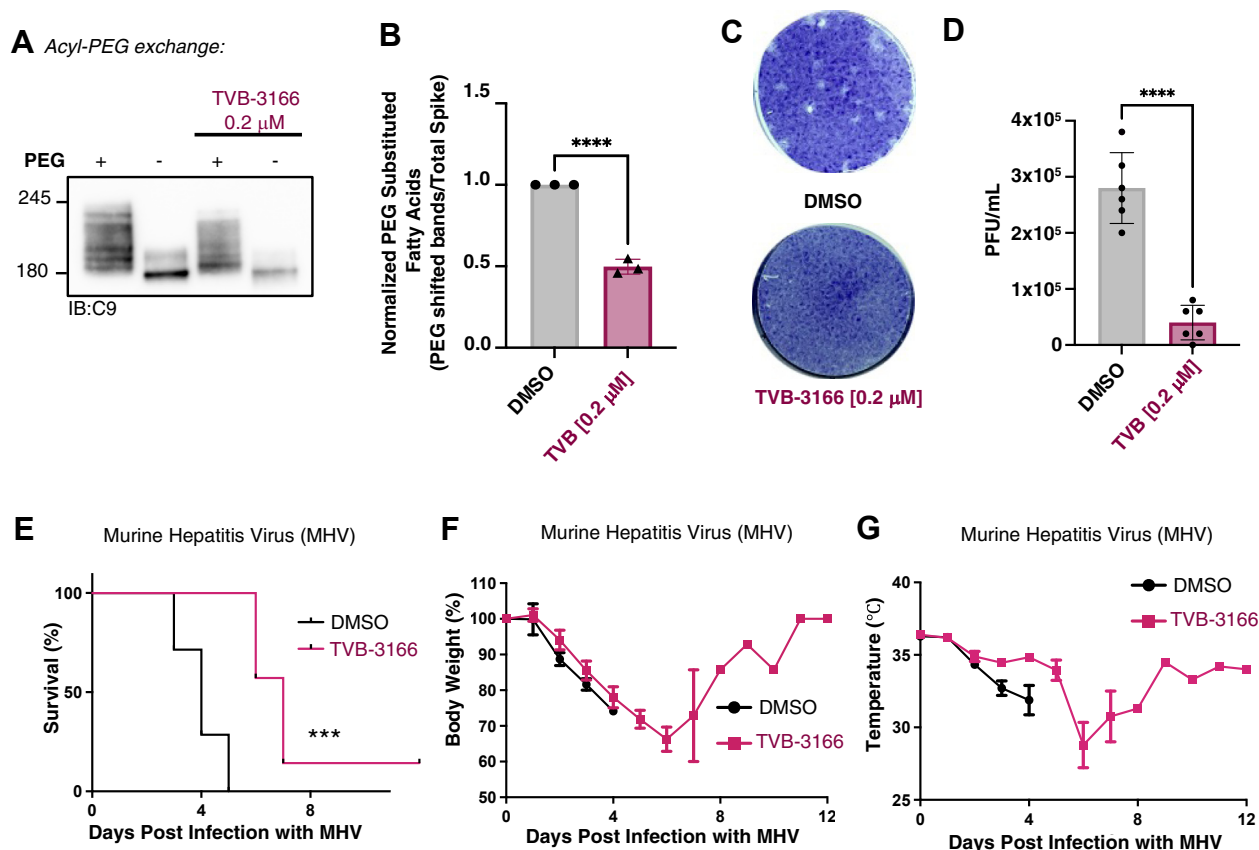


**Fig. 6.** FASN inhibitor TVB-3166 attenuates the virulence of human and murine coronaviruses in vitro and in vivo. A: Acyl-PEG exchange assay and quantification of 229E spike ectopically expressed in HEK293T treated with 0.2  $\mu$ M TVB-3166 for 16–18 h. B: Analysis of acyl-PEG assay where the PEG-modified bands normalized to unmodified bands at ~180 kDa, unpaired *t*-test with Welch's correction; data are mean  $\pm$  SEM of *n* = 3 biological replicates, \*\*\*\**P* < 0.0001. C and D: Plaque assay of MRC-5 cells infected with 229E and treated with 0.2  $\mu$ M TVB-3166 for 4 days, data are mean  $\pm$  SEM of *n* = 3 biological replicates, unpaired *t*-test, \*\*\*\**P* < 0.0001. This image is also included for [supplemental Fig. S5B](#), which demonstrates plaque assays analyzed for this figure. E: Survival of mice challenged by a lethal dose of MHV-S and treated with TVB-3166 (30 mg/kg) following infection (DMSO group: *n* = 7; TVB-3166 group: *n* = 7), survival curves analyzed using a Gehan-Breslow-Wilcoxon test. *P* < 0.005. F and G: Bodyweight and temperature of mice challenged by a lethal dose of MHV-S and treated with TVB-3166 (30 mg/kg) following infection (DMSO group: *n* = 7; TVB-3166 group: *n* = 7). DMSO-treated mice were sacrificed around 4 days p.i. as demonstrated in E. Decisions to sacrifice mice were determined by several health indicators, including body weight and activity.

of post-translational S-acylation for the function of these fusogenic proteins. Collectively, various studies have now found that nearly half of the ZDHHC enzymes have the potential to S-acylate the spike protein. Yet, there are no ZDHHC inhibitors, broad spectrum or selective, in clinical development. However, the findings that FASN inhibitors effectively block S-acylation of SARS-CoV-2 spike protein attenuate the spread of the virus and inhibit the spread of other respiratory viruses (e.g., respiratory syncytial virus, human parainfluenza 3, and rhinovirus) (59) should result in additional studies in the future.

Mechanistically, the techniques that require cleavage of the thioester bond to detect sites of S-acylation, including acyl-biotin exchange, acyl-PEG exchange, and acyl-RAC, do not provide information as to the acyl chain species attached to the Cys residue(s). Using three alkyne-containing fatty acid analogs, we find that clickable analogs of palmitate, myristate, and stearate are attached to the spike protein with a preference for

the 16-carbon analog. We also found that ZDHHC5 has a strong preference for palmitoyl-CoA as a substrate. In collective publications, it has been demonstrated that half the ZDHHC enzymes are capable of modifying the spike protein when they are coexpressed. However, we also find that when spike is expressed in *ZDHHC5* knockouts, the incorporation of palmitate was reduced by 40% suggesting that may play a prominent role at least in some cell types. The recent studies on the S-acylation of the spike protein have relied on a variety of cell lines and techniques to examine post-translational S-acylation. Therefore, the choice of cell types and different techniques may be contributing to the heterogeneity of the collective results. Alternatively, with its 10 Cys residues, it is also conceivable that the spike protein is a promiscuous substrate for the ZDHHC enzymes.

Considering the spike protein contains 10 Cys residues within the C-terminal domain that are proximal to the transmembrane domain, it is worth considering the critical modification sites. A consensus from the various



studies is that Cys1235 and Cys1236 are crucial for the infectivity of both the virus and pseudovirus. In addition, a trend from these studies is that Cys1235, Cys1236, Cys1240, and Cys1241 are sites most highly modified by exogenously added  $^3\text{H}$ -palmitate or the clickable stearate analog 17-ODYA. In addition, the results suggest that Cys1235 and Cys1236 are S-acylated in the endoplasmic reticulum by the ZDHHC20 before transiting to the Golgi apparatus and plasma membrane, where it can encounter additional ZDHHC isoforms. However, these studies rely on the uptake of fatty acids from the medium. The growing body of literature has demonstrated that FASN, and not exogenous fatty acids, is the primary source of acyl chains for S-acylation (25, 54, 60–63). Using an alternative approach, Zeng *et al.* replaced all 10 Cys with alanine residues and subsequently reintroduced individual Cys residues within the tail and examined the S-acylation using the acyl-biotin exchange. This study found that the individual Cys1235, Cys1236, Cys1240, and Cys1241 residues were not being S-acylated in isolation, yet the other six sites were being modified (18). The significance of this finding is currently unclear. Still, it suggests that the recognition of the sites of S-acylation by the ZDHHC is more complex than just their proximity to the transmembrane domain. Another possibility is that thioesterases may more readily recognize some sites, especially in the absence of the other neighboring S-acylated residue, so their steady-state S-acylation may appear lower. Indeed, how a deacylation/reacylation cycle may impact the findings of all these studies should be considered in the future.

This current study, our recent published findings on the peptidoglycan sensors NOD1 and NOD2 (25), and other studies have demonstrated that the inhibition of FASN greatly attenuates the S-acylation of proteins even in the presence of exogenous lipids and lipoproteins (60, 63, 64). Here, we show that FASN inhibition decreases S-acylation of ectopically expressing spike by >95%. The results suggest that exogenous free fatty acids acquired from albumin/medium are not the preferred source for S-acylation at least in the cell types used in our study. Indeed, even under conditions where FASN is completely inhibited, we only see a modest 50% increase in the attachment of the exogenously delivered clickable palmitate to the spike protein. This observation is somewhat unexpected, although, to our knowledge, the source of fatty acids/fatty acyl-CoAs has not been rigorously examined. As such, these findings are significant beyond the study of CoVs and are useful to others studying S-acylation. Treating cells with triacsin C, a molecule known to block fatty acid uptake, does limit the uptake and incorporation of radiolabeled palmitate or clickable fatty acids from the medium (65, 66) as well as prevent the formation of lipid droplets. However, these studies did not investigate whether the proteins were still S-acylated by an independent method like the acyl-biotin exchange. Given

that structurally unrelated FASN inhibitors, including the TVB compounds and cerulenin/C75, and FASN silencing have comparable results, it is unlikely the results are due to off-target effects.

One possible explanation is that exogenously added fatty acids are not internalized and converted to acyl-CoAs efficiently enough to supply the needs of the ZDHHC enzymes. Another possibility is that different acyl-CoA “pools” exist within the cytosol and that these may be channeled for further use and metabolism. Considering acyl-CoAs support phospholipid metabolism, triglyceride synthesis, protein acylation, and can be imported into mitochondria and peroxisomes for beta-oxidation, it may be difficult to resolve this question. In addition, considering the concentration of CoA in the mitochondria is nearly two orders of magnitude higher than the cytosol (67), directly analyzing that cytosolic CoA pools are not trivial. Our findings that the spike protein can also be myristoylated and stearylized (Fig. 3F), yet FASN inhibition abolished S-acylation using the APE assay (Fig. 5D), suggests that the FASN is also critical to generating the CoA species used for these reactions. In support of this notion, two recent studies have found that FASN generates an array of fatty acyl chains beyond just 16:0 and that FASN supports the generation of myristoyl-CoA and stearyl-CoA and their subsequent attachment to proteins (68, 69).


Does the loss of ZDHHC5 and FASN activity impact the SARS-CoV-2 infection cycle by other mechanisms? In all likelihood, yes. First, S-acylation may be important for the function of additional viral proteins. For comparison, the envelope protein of MHV also requires S-acylation to assemble virions (70). Although we did not pick up other SARS-CoV-2 with the acyl-RAC MS analysis, it does not rule out the possibility that other viral proteins are, in fact, S-acylated. Indeed, in a previous study, we found it difficult to detect many of the SARS-CoV-2 proteins, including those that could be potentially S-acylated (33). Second, loss of ZDHHC5 will alter S-acylated proteins at the cell surface, including flotillin, and is also known to increase the rates of two actin-dependent endocytic processes, phagocytosis and macropinocytosis, through an unknown mechanism (25, 27). Considering SARS-CoV-2 is larger than the traditional clathrin-mediated endocytic cargo, other factors such as flotillin or actin machinery may play a role and thus be regulated by ZDHHC5. In addition, since many proteins involved in vesicular transport and membrane fusion are S-acylated (71), including SNAP23 and SNARE proteins, prolonged treatment with FASN inhibitors may also impede vesicular processes and thus attenuate the viral replication cycle. Indeed, small molecules that interfere with phosphoinositides in the endocytic pathway and lysosomal pH are also known to disrupt the viral replication cycle (72–74). Thus, the effects of S-acylation on host cell proteins as well as other viral proteins involved in the

endocytosis, egress, and dissemination of viral particles should be considered in the future.

Alterations in lipid metabolism are documented in CoV infections. Sera from patients with COVID-19 have altered apolipoproteins and lipid levels (75), whereas 229E infected cells have been shown to have increased levels of free fatty acids (75). Given the fact that CoVs are enveloped viruses, they will require host lipids for replication. CoV-induced remodeling of the cellular lipidome is necessary for robust viral replication. Specifically, recent studies have demonstrated that FASN activity is required to support SARS-CoV-2 replication and that blocking fatty acid absorption using orlistat reduced illness and symptoms in mice (73, 76). Additional experiments have demonstrated that the diacylglycerol acyltransferase 1 inhibitor (A922500) attenuates the production of viral progeny (77). This enzyme is critical for lipid droplet formation, and the same study found that SARS-CoV-2 replication centers are in proximity to lipid droplets. Finally, the ectodomain of SARS-CoV-2 spike contains a binding pocket for another fatty acid, linoleic acid (78), although the function is not completely clear. Thus, further studies on the importance of fatty acids and lipid metabolism are needed to clarify these aspects of CoV infections.

Treating cells or mice with TVB-3166 limited the ability of SARS-CoV-2 and 229E to produce virulent progeny and spread in cell culture, and in initial experiments, it extended the life of mice subjected to a lethal MHV infection. We anticipate that our findings will advance the possibility of using the related TVB-2640 to treat COVID-19 or other CoV infections, especially as new variants arise (53, 79). Since FASN is a host enzyme, the likelihood of viral resistance is low. It would necessitate extensive mutagenesis of the spike protein to bypass the requirement for S-acylation of the cytosolic tail to support membrane fusion. Clinically, the identification and approval of an orally available pan-CoV treatment or prophylaxis would be beneficial in the short term and against other zoonotic CoVs in the future.

### Data availability

All MS data have been deposited on Mass Spectrometry Interactive Virtual Environment ([massive.ucsd.edu](https://massive.ucsd.edu)) under accession MSV000088105. All other data are available upon request. 

### Supplemental data

This article contains [supplemental data](#). Five supplementary figures and two supplementary tables are included.

### Acknowledgments

The authors thank the Kennan Research Center for Biomedical Science Core Facilities at St. Michael's Hospital, especially Dr Caterina Di Ciano-Oliveira and Dr Monika Lodyga, for their continued support, technical advice, expertise, and training.

### Author contributions

W. L. L., C. A., B. R., and G. D. F. conceptualization; K. M., M. L., M. S., A. A., J. S.-G., and E. L. methodology; K. M., M. L., M. S., A. A., J. S.-G., E. L., N. K., and K. W. formal analysis; K. M., M. L., M. S., A. A., J. S.-G., E. L., N. K., and K. W. investigation; Z. L. and J. R. resources; K. M. and M. L. writing—original draft; M. S. and G. D. F. writing—review & editing; K. M., M. L., M. S., A. A., J. S.-G., E. L., K. W., and G. D. F. visualization; W. L. L., C. A., B. R., and G. D. F. supervision; W. L., C. A., B. R., and G. D. F. project administration; W. L. L., C. A., B. R., and G. D. F. funding acquisition.

### Author ORCIDs

Warren L. Lee  <https://orcid.org/0000-0002-1788-6587>

Costin Antonescu  <https://orcid.org/0000-0001-9192-6340>

### Funding and additional information

This work was supported by the St. Michael's Hospital Foundation and a Project Grant from the Canadian Institutes of Health Research (grant no.: PJT166010; to G. D. F.). G. D. F. is supported by a Tier 1 Canada Research Chair in Multiomics of Lipids and Innate Immunity. W. L. L. is supported by a Canada Research Chair in Mechanisms of Endothelial Permeability and operating funds from the Keenan Foundation and a Collaborative Health Research Projects grant (grant nos.: CPG 158284; CHRP 523598) from the Canadian Institutes of Health Research/National Sciences and Engineering Research Council. C. A. received funding from the Ryerson Faculty of Science and the Ryerson COVID-19 SRC response fund. M. L. is supported by a doctoral scholarship from the Natural Sciences and Engineering Research Council of Canada. E. L. is supported by a Canadian Graduate Scholarship—master's program and a scholarship from the St. Michael's Hospital Research Training Center.

### Conflict of interest

The patent to TVB-3166 and related compounds belong to Sagimet Biosciences. The authors receive no financial compensation or support from Sagimet Biosciences. The authors do not hold stock or interest in Sagimet Biosciences. The authors declare that they have no conflicts of interest with the contents of this article.

### Abbreviations

ACE2, angiotensin-converting enzyme 2; acyl-RAC, acyl-resin-assisted capture; APE, acyl-polyethylene glycol exchange; CoV, coronavirus; COVID-19, coronavirus disease 2019; Cy5.5, cyanine 5.5; Cys, cysteine; DAPI, 4',6-diamidino-2-phenylindole; D-PBS, Dulbecco's PBS; DSP, dithio-bissuccinimidyl propionate; EMEM, Eagle's MEM; HA, hemagglutinin; 15-HDYA, 15-hexadecynoic acid; HEK293T, human embryonic kidney 293T cell line; MHV, murine hepatitis virus; MOI, multiplicity of infection; NEM, *N*-ethylmaleimide; PEG, polyethylene glycol; PFA, paraformaldehyde; SARS-CoV-2, severe acute respiratory syndrome coronavirus 2; ZDHHC, zinc finger Asp-His-His-Cys.

Manuscript received May 24, 2022, and in revised from July 8, 2022. Published, JLR Papers in Press, July 31, 2022, <https://doi.org/10.1016/j.jlr.2022.100256>

## REFERENCES

- Wang, C., Horby, P. W., Hayden, F. G., and Gao, G. F. (2020) A novel coronavirus outbreak of global health concern. *Lancet* **395**, 470–473
- da Costa, V. G., Moreli, M. L., and Saivish, M. V. (2020) The emergence of SARS, MERS and novel SARS-2 coronaviruses in the 21st century. *Arch. Virol.* **165**, 1517–1526
- To, K. F., Tong, J. H., Chan, P. K., Au, F. W., Chim, S. S., Chan, K. C., *et al.* (2004) Tissue and cellular tropism of the coronavirus associated with severe acute respiratory syndrome: an in-situ hybridization study of fatal cases. *J. Pathol.* **202**, 157–163
- Weiss, S. R., and Leibowitz, J. L. (2011) Coronavirus pathogenesis. *Adv. Virus Res.* **81**, 85–164
- Monteil, V., Kwon, H., Prado, P., Hagelkruys, A., Wimmer, R. A., Stahl, M., *et al.* (2020) Inhibition of SARS-CoV-2 infections in engineered human tissues using clinical-grade soluble human ACE2. *Cell* **181**, 905–913.e907
- Hoffmann, M., Kleine-Weber, H., Schroeder, S., Kruger, N., Herrler, T., Erichsen, S., *et al.* (2020) SARS-CoV-2 cell entry depends on ACE2 and TMPRSS2 and is blocked by a clinically proven protease inhibitor. *Cell* **181**, 271–280.e278
- Kim, Y. C., Dema, B., and Reyes-Sandoval, A. (2020) COVID-19 vaccines: breaking record times to first-in-human trials. *NPJ Vaccin.* **5**, 34
- Hoffmann, M., Kleine-Weber, H., and Pohlmann, S. (2020) A multibasic CLeavage site in the spike protein of SARS-CoV-2 is essential for infection of human lung cells. *Mol. Cell* **78**, 779–784.e775
- Duffy, S., Shackelton, L. A., and Holmes, E. C. (2008) Rates of evolutionary change in viruses: patterns and determinants. *Nat. Rev. Genet.* **9**, 267–276
- Duffy, S. (2018) Why are RNA virus mutation rates so damn high? *PLoS Biol.* **16**, e3000003
- Cui, J., Li, F., and Shi, Z. L. (2019) Origin and evolution of pathogenic coronaviruses. *Nat. Rev. Microbiol.* **17**, 181–192
- Liu, L., Fang, Q., Deng, F., Wang, H., Yi, C. E., Ba, L., *et al.* (2007) Natural mutations in the receptor binding domain of spike glycoprotein determine the reactivity of cross-neutralization between palm civet coronavirus and severe acute respiratory syndrome coronavirus. *J. Virol.* **81**, 4694–4700
- Gordon, D. E., Jang, G. M., Bouhaddou, M., Xu, J., Obernier, K., White, K. M., *et al.* (2020) A SARS-CoV-2 protein interaction map reveals targets for drug repurposing. *Nature* **583**, 459–468
- Puthenveetil, R., Lun, C. M., Murphy, R. E., Healy, L. B., Vilmen, G., Christenson, E. T., *et al.* (2021) S-acylation of SARS-CoV-2 spike protein: mechanistic dissection, in vitro reconstitution and role in viral infectivity. *J. Biol. Chem.* **101112**
- Wu, Z., Zhang, Z., Wang, X., Zhang, J., Ren, C., Li, Y., *et al.* (2021) Palmitoylation of SARS-CoV-2 S protein is essential for viral infectivity. *Signal. Transduct. Target Ther.* **6**, 231
- [preprint] Mesquita, F., Abrami, L., Sergeeva, O., Turelli, P., Kunz, B., Raclot, C., *et al.* (2021) S-acylation controls SARS-CoV-2 membrane lipid organization and enhances infectivity. *BioRxiv*. <https://doi.org/10.1101/2021.03.14.435299>
- Mesquita, F. S., Abrami, L., Sergeeva, O., Turelli, P., Qing, E., Kunz, B., *et al.* (2021) S-acylation controls SARS-CoV-2 membrane lipid organization and enhances infectivity. *Dev. Cell* **56**, 2790–2807.e2798
- Zeng, X. T., Yu, X. X., and Cheng, W. (2021) The interactions of ZDHHC5/GOLGA7 with SARS-CoV-2 spike (S) protein and their effects on S protein's subcellular localization, palmitoylation and pseudovirus entry. *Virol. J.* **18**, 257
- Li, D., Liu, Y., Lu, Y., Gao, S., and Zhang, L. (2022) Palmitoylation of SARS-CoV-2 S protein is critical for S-mediated syncytia formation and virus entry. *J. Med. Virol.* **94**, 342–348
- Ramadan, A. A., Mayilsamy, K., McGill, A. R., Ghosh, A., Giulianotti, M. A., Donow, H. M., *et al.* (2022) Identification of SARS-CoV-2 Spike Palmitoylation Inhibitors That Results in Release of Attenuated Virus with Reduced Infectivity. *Viruses* **14**, 531
- Thorp, E. B., Boscarino, J. A., Logan, H. L., Goletz, J. T., and Gallagher, T. M. (2006) Palmitoylations on murine coronavirus spike proteins are essential for virion assembly and infectivity. *J. Virol.* **80**, 1280–1289
- Shulla, A., and Gallagher, T. (2009) Role of spike protein endodomains in regulating coronavirus entry. *J. Biol. Chem.* **284**, 32725–32734
- Petit, C. M., Chouljenko, V. N., Iyer, A., Colgrove, R., Farzan, M., Knipe, D. M., *et al.* (2007) Palmitoylation of the cysteine-rich endodomain of the SARS-coronavirus spike glycoprotein is important for spike-mediated cell fusion. *Virology* **360**, 264–274
- Li, Z., Tomlinson, A. C., Wong, A. H., Zhou, D., DesForges, M., Talbot, P. J., *et al.* (2019) The human coronavirus HCoV-229E S-protein structure and receptor binding. *Elife* **8**
- Lu, Y., Zheng, Y., Coyaud, E., Zhang, C., Selvabaskaran, A., Yu, Y., *et al.* (2019) Palmitoylation of NOD1 and NOD2 is required for bacterial sensing. *Science* **366**, 460–467
- Korbie, D. J., and Mattick, J. S. (2008) Touchdown PCR for increased specificity and sensitivity in PCR amplification. *Nat. Protoc.* **3**, 1452–1456
- Fekri, F., Abousawan, J., Bautista, S., Orofiamma, L., Dayam, R. M., Antonescu, C. N., *et al.* (2019) Targeted enhancement of flotillin-dependent endocytosis augments cellular uptake and impact of cytotoxic drugs. *Sci. Rep.* **9**, 17768
- Milewska, A., Kaminski, K., Ciejk, J., Kosowicz, K., Zeglen, S., Wojarski, J., *et al.* (2016) HTCC: broad Range Inhibitor of Coronavirus Entry. *PLoS One* **11**, e0156552
- Baer, A., and Kehn-Hall, K. (2014) Viral concentration determination through plaque assays: using traditional and novel overlay systems. *J. Vis. Exp.* <https://doi.org/10.3791/52065>
- Banerjee, A., Nasir, J. A., Budylowski, P., Yip, L., Aftanas, P., Christie, N., *et al.* (2020) Isolation, sequence, infectivity, and replication kinetics of severe acute respiratory syndrome coronavirus 2. *Emerg. Infect. Dis.* **26**, 2054–2063
- De Albuquerque, N., Baig, E., Ma, X., Zhang, J., He, W., Rowe, A., *et al.* (2006) Murine hepatitis virus strain 1 produces a clinically relevant model of severe acute respiratory syndrome in A/J mice. *J. Virol.* **80**, 10382–10394
- Sugiyama, M. G., Armstrong, S. M., Wang, C., Hwang, D., Leong-Poi, H., Advani, A., *et al.* (2015) The Tie2-agonist Vasculotide rescues mice from influenza virus infection. *Sci. Rep.* **5**, 11030
- St-Germain, J. R., Astori, A., and Raught, B. (2021) A SARS-CoV-2 peptide spectral library enables rapid, sensitive identification of virus peptides in complex biological samples. *J. Proteome Res.* **20**, 2187–2194
- Choi, H., Larsen, B., Lin, Z. Y., Breitkreutz, A., Mellacheruvu, D., Fermin, D., *et al.* (2011) SAINT: probabilistic scoring of affinity purification-mass spectrometry data. *Nat. Met.* **8**, 70–73
- Molday, L. L., and Molday, R. S. (2014) ID4: a versatile epitope tag for the purification and characterization of expressed membrane and soluble proteins. *Met. Mol. Biol.* **1177**, 1–15
- Shang, J., Ye, G., Shi, K., Wan, Y., Luo, C., Aihara, H., *et al.* (2020) Structural basis of receptor recognition by SARS-CoV-2. *Nature* **581**, 221–224
- Ou, X., Liu, Y., Lei, X., Li, P., Mi, D., Ren, L., *et al.* (2020) Characterization of spike glycoprotein of SARS-CoV-2 on virus entry and its immune cross-reactivity with SARS-CoV. *Nat. Commun.* **11**, 1620
- Gaebler, A., Milan, R., Straub, L., Hoelper, D., Kuerschner, L., and Thiele, C. (2013) Alkyne lipids as substrates for click chemistry-based in vitro enzymatic assays. *J. Lipid Res.* **54**, 2282–2290
- Tornøe, C. W., Christensen, C., and Meldal, M. (2002) Peptidotriazoles on solid phase: [1,2,3]-triazoles by regioselective copper(I)-catalyzed 1,3-dipolar cycloadditions of terminal alkynes to azides. *J. Org. Chem.* **67**, 3057–3064
- Rostovtsev, V. V., Green, L. G., Fokin, V. V., and Sharpless, K. B. (2002) A stepwise Huisgen cycloaddition process: copper(I)-catalyzed regioselective "ligation" of azides and terminal alkynes. *Angew. Chem. Int. Ed. Engl.* **41**, 2596–2599
- Charron, G., Zhang, M. M., Yount, J. S., Wilson, J., Raghavan, A. S., Shamir, E., *et al.* (2009) Robust fluorescent detection of protein fatty-acylation with chemical reporters. *J. Am. Chem. Soc.* **131**, 4967–4975
- Percher, A., Ramakrishnan, S., Thion, E., Yuan, X., Yount, J. S., and Hang, H. C. (2016) Mass-tag labeling reveals site-specific and endogenous levels of protein S-fatty acylation. *Proc. Natl. Acad. Sci. U. S. A.* **113**, 4302–4307
- Forrester, M. T., Hess, D. T., Thompson, J. W., Hultman, R., Moseley, M. A., Stamler, J. S., *et al.* (2011) Site-specific analysis of protein S-acylation by resin-assisted capture. *J. Lipid Res.* **52**, 393–398



44. Abe, K. T., Li, Z., Samson, R., Samavarchi-Tehrani, P., Valcourt, E. J., Wood, H., *et al.* (2020) A simple protein-based surrogate neutralization assay for SARS-CoV-2. *JCI Insight* **5**, e142362
45. Bosch, B. J., van der Zee, R., de Haan, C. A., and Rottier, P. J. (2003) The coronavirus spike protein is a class I virus fusion protein: structural and functional characterization of the fusion core complex. *J. Virol.* **77**, 8801–8811
46. Cattin-Ortola, J., Welch, L. G., Maslen, S. L., Papa, G., James, L. C., and Munro, S. (2021) Sequences in the cytoplasmic tail of SARS-CoV-2 Spike facilitate expression at the cell surface and syncytia formation. *Nat. Commun.* **12**, 5333
47. Jennings, B. C., and Linder, M. E. (2012) DHHC protein S-acyltransferases use similar ping-pong kinetic mechanisms but display different acyl-CoA specificities. *J. Biol. Chem.* **287**, 7236–7245
48. Nomura, R., Kiyota, A., Suzuki, E., Kataoka, K., Ohe, Y., Miyamoto, K., *et al.* (2004) Human coronavirus 229E binds to CD13 in rafts and enters the cell through caveolae. *J. Virol.* **78**, 8701–8708
49. Loftus, T. M., Jaworsky, D. E., Frehywot, G. L., Townsend, C. A., Ronnett, G. V., Lane, M. D., *et al.* (2000) Reduced food intake and body weight in mice treated with fatty acid synthase inhibitors. *Science* **288**, 2379–2381
50. Montesdeoca, N., Lopez, M., Ariza, X., Herrero, L., and Makowski, K. (2020) Inhibitors of lipogenic enzymes as a potential therapy against cancer. *FASEB J.* **34**, 11355–11381
51. Flavin, R., Peluso, S., Nguyen, P. L., and Loda, M. (2010) Fatty acid synthase as a potential therapeutic target in cancer. *Future Oncol.* **6**, 551–562
52. Singh, S., Karthikeyan, C., and Moorthy, N. (2020) Recent advances in the development of fatty acid synthase inhibitors as anticancer agents. *Mini Rev. Med. Chem.* **20**, 1820–1837
53. Syed-Abdul, M. M., Parks, E. J., Gaballah, A. H., Bingham, K., Hammoud, G. M., Kembler, G., *et al.* (2020) Fatty acid synthase inhibitor TVB-2640 reduces hepatic de novo lipogenesis in males with metabolic abnormalities. *Hepatology* **72**, 103–118
54. Heuer, T. S., Ventura, R., Mordec, K., Lai, J., Fridlib, M., Buckley, D., *et al.* (2017) FASN inhibition and taxane treatment combine to enhance anti-tumor efficacy in diverse xenograft tumor models through disruption of tubulin palmitoylation and microtubule organization and FASN inhibition-mediated effects on oncogenic signaling and gene expression. *EBioMedicine* **16**, 51–62
55. Ventura, R., Mordec, K., Waszczuk, J., Wang, Z., Lai, J., Fridlib, M., *et al.* (2015) Inhibition of de novo palmitate synthesis by fatty acid synthase induces apoptosis in tumor cells by remodeling cell membranes, inhibiting signaling pathways, and reprogramming gene expression. *EBioMedicine* **2**, 808–824
56. Davda, D., El Azzouny, M. A., Tom, C. T., Hernandez, J. L., Majumdar, J. D., Kennedy, R. T., *et al.* (2013) Profiling targets of the irreversible palmitoylation inhibitor 2-bromopalmitate. *ACS Chem. Biol.* **8**, 1912–1917
57. Loomba, R., Mohseni, R., Lucas, K. J., Gutierrez, J. A., Perry, R. G., Trotter, J. F., *et al.* (2021) TVB-2640 (FASN Inhibitor) for the treatment of nonalcoholic steatohepatitis: FASCINATE-1, a randomized, placebo-controlled phase 2a trial. *Gastroenterology* **161**, 1475–1486
58. Falchook, G., Infante, J., Arkenau, H. T., Patel, M. R., Dean, E., Borazanci, E., *et al.* (2021) First-in-human study of the safety, pharmacokinetics, and pharmacodynamics of first-in-class fatty acid synthase inhibitor TVB-2640 alone and with a taxane in advanced tumors. *EClinicalMedicine* **34**, 100797
59. Ohol, Y. M., Wang, Z., Kembler, G., and Duke, G. (2015) Direct inhibition of cellular fatty acid synthase impairs replication of respiratory syncytial virus and other respiratory viruses. *PLoS One* **10**, e0144648
60. Kim, Y. C., Lee, S. E., Kim, S. K., Jang, H. D., Hwang, I., Jin, S., *et al.* (2019) Toll-like receptor mediated inflammation requires FASN-dependent MYD88 palmitoylation. *Nat. Chem. Biol.* **15**, 907–916
61. Jochen, A. L., Hays, J., and Mick, G. (1995) Inhibitory effects of cerulenin on protein palmitoylation and insulin internalization in rat adipocytes. *Biochim. Biophys. Acta* **1259**, 65–72
62. Xiong, W., Sun, K. Y., Zhu, Y., Zhang, X., Zhou, Y. H., and Zou, X. (2021) Metformin alleviates inflammation through suppressing FASN-dependent palmitoylation of Akt. *Cell Death Dis.* **12**, 934
63. Wei, X., Schneider, J. G., Shenouda, S. M., Lee, A., Towler, D. A., Chakravarthy, M. V., *et al.* (2011) De novo lipogenesis maintains vascular homeostasis through endothelial nitric-oxide synthase (eNOS) palmitoylation. *J. Biol. Chem.* **286**, 2933–2945
64. Wei, X., Yang, Z., Rey, F. E., Ridaura, V. K., Davidson, N. O., Gordon, J. I., *et al.* (2012) Fatty acid synthase modulates intestinal barrier function through palmitoylation of mucin 2. *Cell Host Microbe* **11**, 140–152
65. Weis, M. T., Crumley, J. L., Young, L. H., and Stallone, J. N. (2004) Inhibiting long chain fatty Acyl CoA synthetase increases basal and agonist-stimulated NO synthesis in endothelium. *Cardiovasc. Res.* **63**, 338–346
66. Kilian, N., Zhang, Y., LaMonica, L., Hooker, G., Toomre, D., Mamoun, C. B., *et al.* (2020) Palmitoylated proteins in plasmodium falciparum-infected erythrocytes: investigation with click chemistry and metabolic labeling. *Bioessays* **42**, e1900145
67. Leonardi, R., Zhang, Y. M., Rock, C. O., and Jackowski, S. (2005) Coenzyme A: back in action. *Prog. Lipid Res.* **44**, 125–153
68. Karthikeyan, K. P., Zhang, L., Loisele, D. R., Haystead, T. A. J., Bhat, M., Yount, J. S., *et al.* (2021) A bioorthogonal chemical reporter for fatty acid synthase-dependent protein acylation. *J. Biol. Chem.* **297**, 101272
69. Topolska, M., Martinez-Montanes, F., and Ejsing, C. S. (2020) A simple and direct assay for monitoring fatty acid synthase activity and product-specificity by high-resolution mass spectrometry. *Biomolecules* **10**, 118
70. Boscarino, J. A., Logan, H. L., Lacny, J. J., and Gallagher, T. M. (2008) Envelope protein palmitoylations are crucial for murine coronavirus assembly. *J. Virol.* **82**, 2989–2999
71. Dixon, C. L., Mekhail, K., and Fairn, G. D. (2021) Examining the Underappreciated Role of S-Acylated Proteins as Critical Regulators of Phagocytosis and Phagosome Maturation in Macrophages. *Front. Immunol.* **12**, 659533
72. Kang, Y. L., Chou, Y. Y., Rothlauf, P. W., Liu, Z., Soh, T. K., Cureton, D., *et al.* (2020) Inhibition of PIKfyve kinase prevents infection by Zaire ebolavirus and SARS-CoV-2. *Proc. Natl. Acad. Sci. U. S. A.* **117**, 20803–20813
73. Williams, C. G., Jureka, A. S., Silvas, J. A., Nicolini, A. M., Chvatal, S. A., Carlson-Stevermer, J., *et al.* (2021) Inhibitors of VPS34 and fatty-acid metabolism suppress SARS-CoV-2 replication. *Cell Rep.* **36**, 109479
74. Sauvat, A., Ciccocanti, F., Colavita, F., Di Rienzo, M., Castilletti, C., Capobianchi, M. R., *et al.* (2020) On-target versus off-target effects of drugs inhibiting the replication of SARS-CoV-2. *Cell Death Dis.* **11**, 656
75. Shen, B., Yi, X., Sun, Y., Bi, X., Du, J., Zhang, C., *et al.* (2020) Proteomic and Metabolomic Characterization of COVID-19 Patient Sera. *Cell* **182**, 59–72.e15
76. Chu, J., Xing, C., Du, Y., Duan, T., Liu, S., Zhang, P., *et al.* (2021) Pharmacological inhibition of fatty acid synthesis blocks SARS-CoV-2 replication. *Nat. Metab.* **3**, 1466–1475
77. Dias, S. S. G., Soares, V. C., Ferreira, A. C., Sacramento, C. Q., Fintelman-Rodrigues, N., Temerozo, J. R., *et al.* (2020) Lipid droplets fuel SARS-CoV-2 replication and production of inflammatory mediators. *PLoS Pathog.* **16**, e1009127
78. Toelzer, C., Gupta, K., Yadav, S. K. N., Borucu, U., Davidson, A. D., Kavanagh Williamson, M., *et al.* (2020) Free fatty acid binding pocket in the locked structure of SARS-CoV-2 spike protein. *Science* **370**, 725–730
79. Jones, S. F., and Infante, J. R. (2015) Molecular Pathways: fatty Acid Synthase. *Clin. Cancer Res.* **21**, 5434–5438